Supporting Information

Chemically Regulating Rh(I)-Bodipy Photoredox Switches

A. M. Lifschitz,[a] R. M. Young,[a,b] J. Mendez-Arroyo,[a] V. V. Roznyatovskiy,[a,b] C. M. McGuirk,[a] M. R. Wasielewski[a,b] and C. A. Mirkin[a]

[a] Department of Chemistry and International Institute for Nanotechnology, Northwestern University, 2145 Sheridan Road, Evanston, Illinois 60208, United States.

[b] Argonne-Northwestern Solar Energy Research (ANSER) Center, Northwestern University, Evanston, Illinois 60208, United States.

Table of Contents

Experimental

Materials and Methods. All ligands were synthesized and stored using standard Schlenk line conditions, under an inert nitrogen atmosphere. Phosphinoalkylthiol-Bodipy ligand **S3**,[1] benzyl-(2-diphenylphosphinoethyl)thioether[2] and (2-diphenylphosphinoethyl)-diphenylamine[3] were synthesized as reported previously in the literature. The synthesis and manipulation of all Rh(I) complexes was performed in an inert-atmosphere glove box. All solvents were purchased as HPLC grade and degassed thoroughly under a stream of argon previous to use. Deuterated solvents were purchased from Cambridge Isotope Laboratories and degassed under a stream of argon prior to use. All other chemicals were purchased from Aldrich Chemical Co. and used as received. NMR spectra were recorded on a Bruker Avance 400 MHz. ^{1}H and $^{13}C\{^{1}H\}$ NMR spectra were referenced to residual proton and carbon resonances in the deuterated solvents. $^{31}P\{^{1}H\}$ NMR spectra were referenced to an 85% H_3PO_4 aqueous solution. ^{19}F NMR spectra were referenced to a $CFCl_3$ sample in $CDCl_3$ solution. $^{11}B\{^{1}H\}$ NMR spectra were referenced to neat $BF_3{\bullet}OEt_2$. All chemical shifts are reported in ppm. High Resolution electrospray ionization (ESI) mass spectra measurements were recorded on an Agilent 6120 LC-TOF instrument in positive ion mode.

UV-vis absorption measurements were performed in a Varian Cary 50 Bio spectrophotometer utilizing 10 mm cell-path quartz cuvettes (VWR). fluorescence emission and fluorescence excitation measurements were carried out in a Horiba Jovin-Yvonne Fluorolog fluorimeter and fluorescence quantum yields were derived from the comparative method using sulforhodamine B or fluorescein isothiocyanate in ethanol as standards. In particular, quantum yields were calculated from the least squares fit of integrated fluorescence emission versus absorbance values curves comprising seven dilution samples.

Electrochemical measurements were performed with an Epsilon BASi potentiostat. Cyclic voltammetry measurements were recorded in an air-tight cell comprising a glassy carbon working electrode, a Ag wire pseudo-reference electrode and a Pt wire auxiliary electrode. Samples were prepared in an inert atmosphere glove box as 5 mM solution in 0.1 M n-Bu_4NPF_6 in CH_2Cl_2. Scan rates of 100 mV/s were

used in all measurements. All cyclic voltammetry graphs show voltages versus the ferrocene/ferrocenium couple. Spectroelectrochemical measurements were performed in an air-tight, 2 mm cuvette incorporating a Pt mesh working electrode, a Ag wire pseudo-reference electrode and a Pt wire auxiliary electrode, and spectral changes were recorded in a Varian Cary 50 Bio spectrophotometer.

Transient Absorption Spectroscopy. Visible/near-infrared femtosecond transient absorption spectroscopy was performed on an instrument that is described elsewhere.[4] Briefly, the 827 nm fundamental output of a commercial Ti:sapphire laser system (Tsunami oscillator / Spitfire amplifier, Spectra-Physics) is frequency doubled to 414 nm (~150 μJ/pulse). Depending on the desired pump wavelength, this light is either attenuated and used directly for sample excitation or it used to pump a seeded, two-stage, laboratory-constructed optical parametric amplifier (OPA); in both cases it is then chopped at 500 Hz and rotated to be at the magic angle (54.7º) to the probe. The single-filament continuum probe is generated by focusing into the appropriate non-linear medium for the desired probe range. For visible continuum (430–850 nm), ~1.5 μJ/pulse is tightly focused into a 3 mm sapphire plate, while for the NIR probe (800–1600 nm), ~5 μJ/pulse is loosely focused into a proprietary source (Ultrafast Systems, LLC). Both pump and probe are focused to ~100 μm at the sample. After interaction, the transmitted probe is then coupled into an optical fiber and detected using the appropriate detector (customized Helios, Ultrafast Systems, LLC).

General Procedure for the Generation of Rh(I) complexes. All Rh(I) complexes were first prepared as chloride salts via dropwise addition of a solution of benzyl-(2-diphenylphosphinoethyl)thioether (33.6 mg, 0.100 mmol) in 5 mL of CH_2Cl_2 to a solution of Rh_2Cl_2 (cyclooctene)$_4$ (35.9 mg, 0.100 mmol) in 5 mL of CH_2Cl_2. After stirring for 5 minutes, a solution of the second ligand ligand (0.100 mmol) in 5 mL of CH_2Cl_2 was added in a dropwise fashion. The solution volume was then reduced to approximately 1 mL and the product was precipitated with pentane. The product was collected *via* vacuum filtration and washed with pentane to afford the semiopen complex (*in situ* $^{31}P\{^1H\}$ NMR yields = quantitative, isolated yields >95%). In the case of complexes **1** and **S1**, multiple recrystallizations from CH2Cl2/pentane

mixtures were required to isolate the semiopen heteroligated product, generally afforded in 60-70% yield depending on recrystallization conditions.

Chloride abstraction was achieved via suspension of 2 eq. of Tl(OTf) (70.7 mg, 0.200 mmol) in 3 mL of CH_2Cl_2 solution of the semiopen complexes (0.100 mmol). Complex **S4** was synthesized via chloride abstraction with $TlBF_4$. In all cases, the suspension was filtered through a pad of Celite after 20 minutes of vigorous stirring and the sample was recrystallized from a CH_2Cl_2/pentane mixture to afford the corresponding closed complexes (*in situ* $^{31}P\{^1H\}$ NMR yields = quantitative, isolated yields >95%). Closed complexes were quantitatively converted back to their chloride salts via addition of n-Bu_4NCl (24.5 mg, 0.100 mmol) to a CH_2Cl_2 solution of closed complex (0.100 mmol). Partial displacement of phosphinoalkylamino ligands in closed complexes with a neutral moiety was achieved via the addition of 50 µl of acetonitrile to a 3 ml solution of closed complex (0.100 mmol) in CH_2Cl_2 (*in situ* $^{31}P\{^1H\}$ NMR yields = quantitative). The acetonitrile-coordinated complexes were converted back to their closed complex counterparts through removal of all solvent in vacuo and re-dissolution in CH_2Cl_2 (*in situ* $^{31}P\{^1H\}$ NMR yields = quantitative, isolated yields >98%).

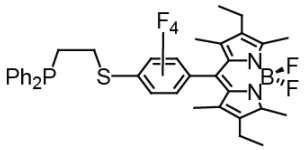

Figure S1. Previously reported ligand **S3** used in the formation of complexes **1** and **2**.[1]

[RhCl(κ$_2$-P,S-Bz)(P,S-F$_4$ph-Bodipy)] (1). ^1H NMR (400.16 MHz, 25˚C, CD_2Cl_2): δ 7.68-7.07 (m, 25 H), 4.03-0.97 (m, 32 H). $^{31}P\{^1H\}$ NMR (161.98 MHz, 25˚C, CD_2Cl_2): δ 70.9 (dd, J_{P-P} = 40 Hz, J_{P-Rh} = 185 Hz, 1 P), 31.0 (dd, J_{P-P} = 40 Hz, J_{P-Rh} = 167 Hz, 1 P). ^{19}F NMR (376.49 MHz, 25˚C, CD_2Cl_2): δ -132.0 (m, 2 F), -141.4 (m, 2 F), -146.0 (q, J_{F-B} = 33 Hz, 2 F). $^{11}B\{^1H\}$ NMR (128.38 MHz, 25˚C, CD_2Cl_2): δ 0.05 (t, J_{B-F} = 33 Hz). HRMS (ESI+) *m/z* calcd for $[M+H]^+$: 1171.2257; found: 1171.2262.

[Rh(κ$_2$-P,S-Bz)(κ$_2$-P,S-F$_4$ph-Bodipy)]OTf (2). ^{1}H NMR (400.16 MHz, 25˚C, CD_2Cl_2): δ 8.30-6.40 (m, 25 H), 4.21-0.80 (m, 32 H). ^{31}P{^{1}H} NMR (161.98 MHz, 25˚C, CD_2Cl_2): δ 64.3 (dd, J_{P-P} = 35 Hz, J_{P-Rh} = 88 Hz, 1 P), 63.3 (dd, J_{P-P} = 35 Hz, J_{P-Rh} = 96 Hz, 1 P). ^{19}F NMR (376.49 MHz, 25˚C, CD_2Cl_2): δ -78.9 (s, 3 F), -128.7 (m, 2 F), -136.9 (m, 2 F), -145.7 (q, J_{F-B} = 31 Hz, 2 F). ^{11}B{^{1}H} NMR (128.38 MHz, 25˚C, CD_2Cl_2): δ 0.40 (t, J_{B-F} = 33 Hz). HRMS (ESI+) *m/z* calcd for [M-OTf]$^+$: 1135.2491; found: 1135.2514.

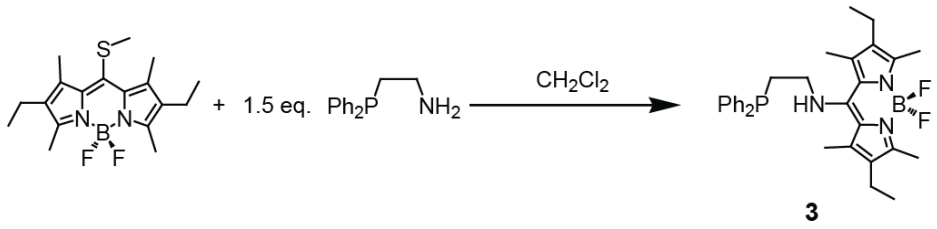

Figure S2. Synthesis of ligand **3**.

P,N(H)-Bodipy (3). 8-thiomethyl-Bodipy **S6** (809 mg, 2.30 mmol) was dissolved in 10 ml of anhydrous CH_2Cl_2 in a Schlenk flask and 2-(diphenylphosphino)ethylamine (1.5 eq., 834 mg, 3.64 mmol) in 2 ml of CH_2Cl_2 was added. After two days of stirring at room temperature the solvent was removed in vacuo. The crude product was re-dissolved in a 1:1 mixture of CH_2Cl_2/hexanes and passed through a silica plug. The orange eluate was collected and the solvent was evacuated in vacuo. The product was then recrystallized from a CH_2Cl_2/ether mixture to afford an orange crystalline solid (1.068 g, 2.01 mmol, 87% yield). ^{1}H NMR (400.16 MHz, 25˚C, CD_2Cl_2): δ 7.38-7.33 (m, 10 H), 5.75 (br s, 1 H), 3.60 (m, 2H), 2.42 (br s, 12H), 2.24 (s, 6 H), 1.04 (t, J_{H-H} = 7 Hz, 8 H). ^{13}C{^{1}H} (100.63 MHz, 25˚C, CD_2Cl_2): δ 150.7 (s), 144.9 (s), 136.8 (d, J_{C-P} = 11 Hz), 132.7 (d, J_{C-P} = 19 Hz), 129.8 (s), 129.0 (s), 129.0 (s), 128.7 (s), 128.6 (s), 122.8 (s), 49.2 (d, J_{C-P} = 6 Hz), 30.8 (d, J_{C-P} = 15 Hz), 17.1 (s) , 14.7 (s) , 13.0 (s) , 11.7 (s). ^{31}P{^{1}H} NMR (161.98 MHz, 25˚C, CD_2Cl_2): δ -22.2 (s). ^{19}F NMR (376.49 MHz, 25˚C, CD_2Cl_2): δ -145.5 (q, J_{F-B} = 34 Hz). ^{11}B{^{1}H} NMR (128.38 MHz, 25˚C, CD_2Cl_2): δ 0.59 (t, J_{B-F} = 33 Hz). HRMS (ESI+) *m/z* calcd for [M+H]$^+$: 532.2864; found: 532.2865.

[Rh(κ$_2$-P,S-Bz)(κ$_2$-P,N(H)-Bodipy)]OTf (4). ^{1}H NMR (400.16 MHz, 25˚C, CD_2Cl_2): δ 7.45-6.54 (m, 25 H), 3.49-0.80 (m, 33 H). ^{31}P{^{1}H} NMR (161.98 MHz, 25˚C, CD_2Cl_2): δ 66.7 (dd, J_{P-P} = 38 Hz, J_{P-Rh} =

179 Hz, 1 P), 50.0 (dd, J_{P-P} = 38 Hz, J_{P-Rh} = 166 Hz, 1 P). ^{19}F NMR (376.49 MHz, 25˚C, CD_2Cl_2): δ -79.2 (s, 3 F), -145.7 (m, 2 F). ^{11}B{^{1}H} NMR (128.38 MHz, 25˚C, CD_2Cl_2): δ -0.02 (t, J_{B-F} = 33 Hz). HRMS (ESI+) *m/z* calcd for $[M-OTf]^+$: 970.2943; found: 970.2940.

[Rh(κ$_2$-P,S-Bz)(P,N(H)-Bodipy)(CH$_3$CN)]OTf (5). ^{1}H NMR (400.16 MHz, 25˚C, CD_2Cl_2): δ 7.63-5.90 (m, 25 H), 4.26-0.89 (m, 32 H). ^{31}P{^{1}H} NMR (161.98 MHz, 25˚C, CD_2Cl_2): δ 68.6 (dd, J_{P-P} = 45 Hz, J_{P-Rh} = 173 Hz, 1 P), 25.2 (dd, J_{P-P} = 45 Hz, J_{P-Rh} = 160 Hz, 1 P). ^{19}F NMR (376.49 MHz, 25˚C, CD_2Cl_2): δ -79.2 (s, 3 F), -144.7 (q, J_{F-B} = 31 Hz, 2 F). ^{11}B{^{1}H} NMR (128.38 MHz, 25˚C, CD_2Cl_2): δ -0.32 (t, J_{B-F} = 32 Hz). HRMS (ESI+) *m/z* calcd for $[M-OTf]^+$: 1011.3208; found: 1011.3192.

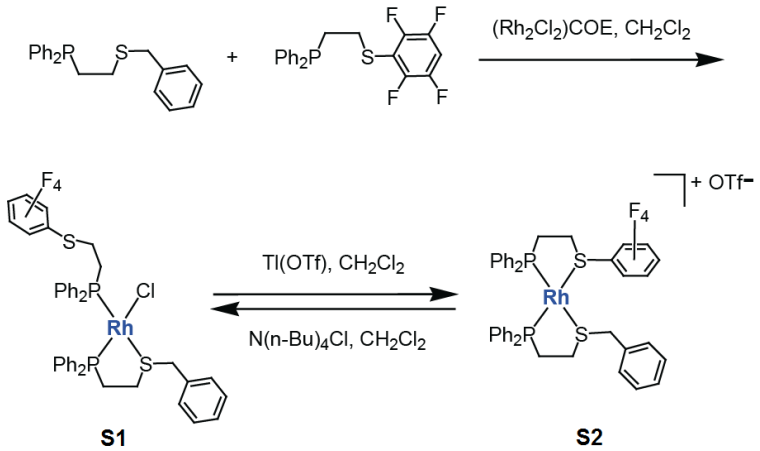

Figure S3. Synthesis of complexes **S1** and **S2** which mimic the coordination environment of **1** and **2**.

[RhCl(κ$_2$-P,S-Bz)(P,S-F$_4$ph)] (S1). ^{1}H NMR (400.16 MHz, 25˚C, CD_2Cl_2): δ 8.20-6.60 (m, 25 H), 4.23-0.88 (m, 10 H). ^{31}P{^{1}H} NMR (161.98 MHz, 25˚C, CD_2Cl_2): δ 70.5 (dd, J_{P-P} = 41 Hz, J_{P-Rh} = 185 Hz, 1 P), 31.2 (dd, J_{P-P} = 41 Hz, J_{P-Rh} = 166 Hz, 1 P). ^{19}F NMR (376.49 MHz, 25˚C, CD_2Cl_2): δ -134.4 (m, 2 F), -139.4 (m, 2 F). HRMS (ESI+) *m/z* calcd for $[M+H]^+$: 869.0491; found: 869.0472.

[Rh(κ$_2$-P,S-Bz)(κ$_2$-P,S-F$_4$ph)]OTf (S2). ^{1}H NMR (400.16 MHz, 25˚C, CD_2Cl_2): δ 8.30-6.40 (m, 26 H), 4.29-0.88 (m, 10 H). ^{31}P{^{1}H} NMR (161.98 MHz, 25˚C, CD_2Cl_2): δ 63.9 (dd, J_{P-P} = 28 Hz, J_{P-Rh} = 165 Hz, 1 P), 63.5 (dd, J_{P-P} = 18 Hz, J_{P-Rh} = 165 Hz, 1 P). ^{19}F NMR (376.49 MHz, 25˚C, CD_2Cl_2): δ -77.7 (s, 3 F), -130.0 (m, 2 F), -134.3 (m, 2 F). HRMS (ESI+) *m/z* calcd for $[M-OTf]^+$: 833.0725; found: 833.0705.

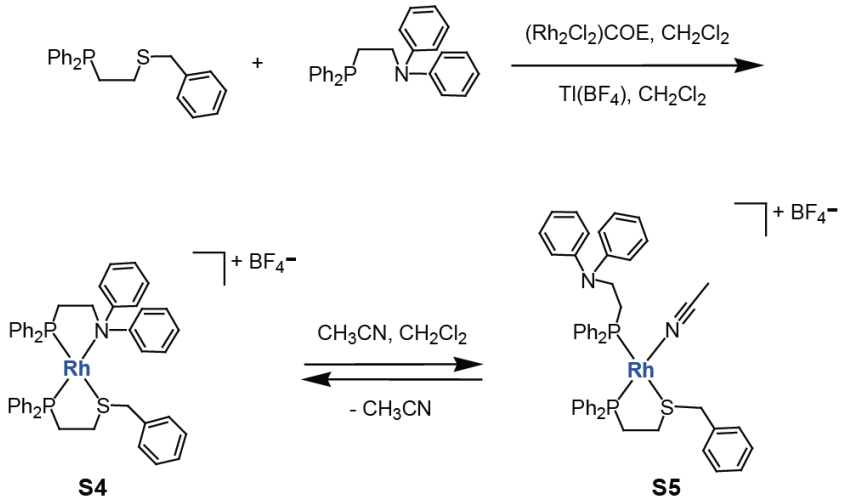

Figure S4. Synthesis of complexes **S4** and **S5** which mimic the coordination environment of **4** and **5**.

[Rh(κ$_2$-P,S-Bz)(κ$_2$-P,N(ph)$_2$)]BF$_4$ (S4). ^{1}H NMR (400.16 MHz, 25˚C, CD_2Cl_2): δ 8.40-6.10 (m, 35 H), 4.40-0.75 (m, 21 H). ^{31}P{^{1}H} NMR (161.98 MHz, 25˚C, CD_2Cl_2): δ 65.7 (dd, J_{P-P} = 42 Hz, J_{P-Rh} = 178 Hz, 1 P), 48.4 (dd, J_{P-P} = 42 Hz, J_{P-Rh} = 173 Hz, 1 P). ^{19}F NMR (376.49 MHz, 25˚C, CD_2Cl_2): δ -153.7 (s). ^{11}B{^{1}H} NMR (128.38 MHz, 25˚C, CD_2Cl_2): δ -1.29 (s). HRMS (ESI+) *m/z* calcd for $[M-BF_4]^+$: 820.1803; found: 820.1780.

[Rh(κ$_2$-P,S-Bz)(P,N(ph)$_2$)(CH$_3$CN)]BF$_4$ (S5). ^{1}H NMR (400.16 MHz, 25˚C, CD_2Cl_2): δ 8.30-6.30 (m, 35 H), 4.30-3.56 (m, 6 H), 2.31-1.25 (m, 21 H). ^{31}P{^{1}H} NMR (161.98 MHz, 25˚C, CD_2Cl_2): δ 69.5 (dd, J_{P-P} = 43 Hz, J_{P-Rh} = 142 Hz, 1 P), 24.4 (dd, J_{P-P} = 44 Hz, J_{P-Rh} = 164 Hz, 1 P). ^{19}F NMR (376.49 MHz, 25˚C, CD_2Cl_2): δ -153.6 (s). ^{11}B{^{1}H} NMR (128.38 MHz, 25˚C, CD_2Cl_2): δ -1.32 (s). HRMS (ESI+) *m/z* calcd for $[M-BF_4]^+$: 861.2068; found: 861.2049.

Absorption Spectra

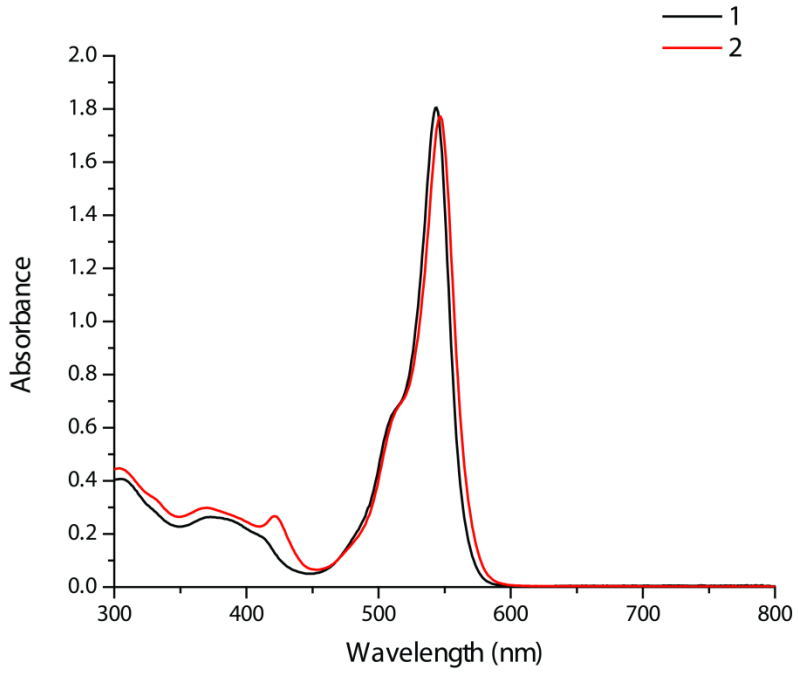

Figure S5. Absorption spectra of 25 μM solutions of complexes **1** and **2** in CH_2Cl_2.

Fluorescence Emission Spectra

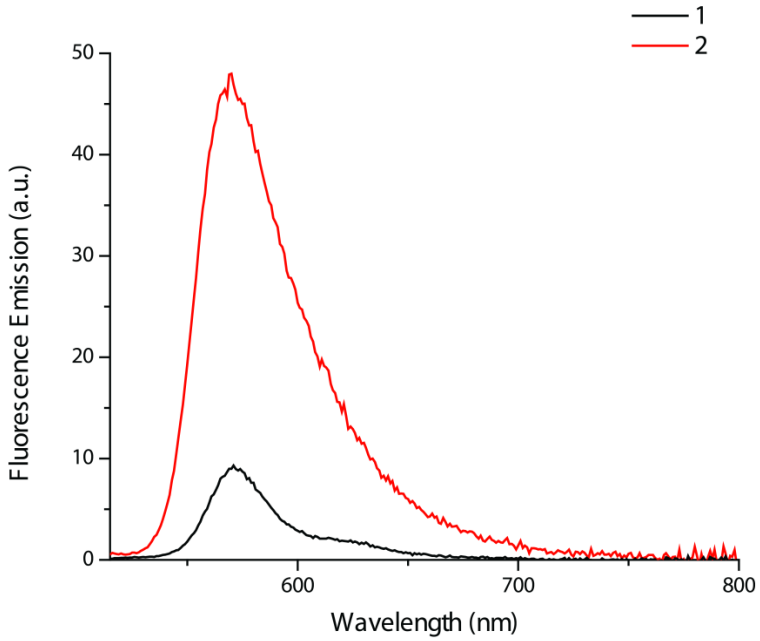

Figure S6. Fluorescence Emission spectra of complexes **1** and **2** in CH_2Cl_2 normalized to reflect their relative fluorescence quantum yield values (λ_{ex} = 505 nm).

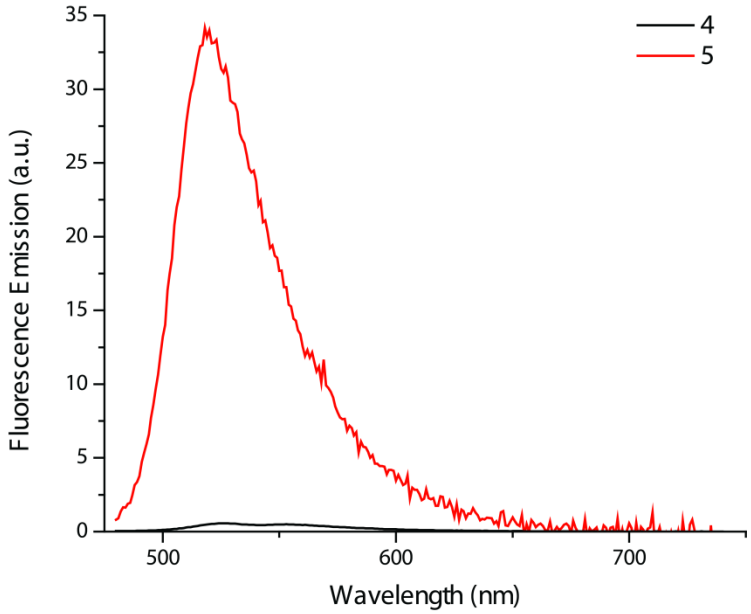

Figure S7. Fluorescence Emission spectra of equimolar solutions of complexes **4** and **5** in CH_2Cl_2 normalized to reflect their relative fluorescence emission intensities (λ_{ex} = 470 nm).

Excitation Spectra

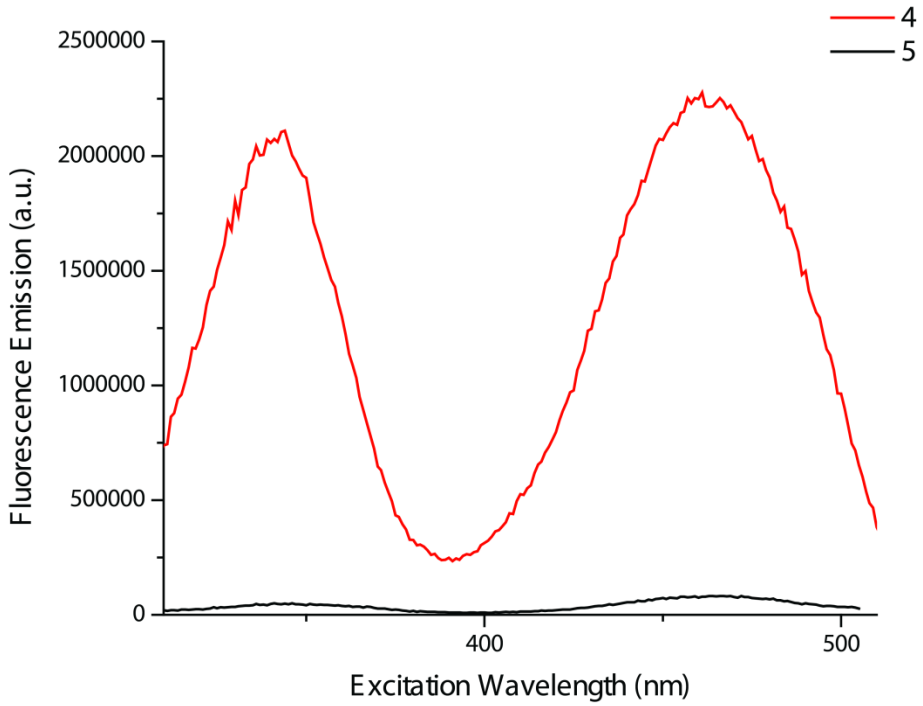

Figure S8. Fluorescence excitation spectra of **4** and **5** in CH_2Cl_2 (λ_{emm} = 520 nm).

Electrochemistry

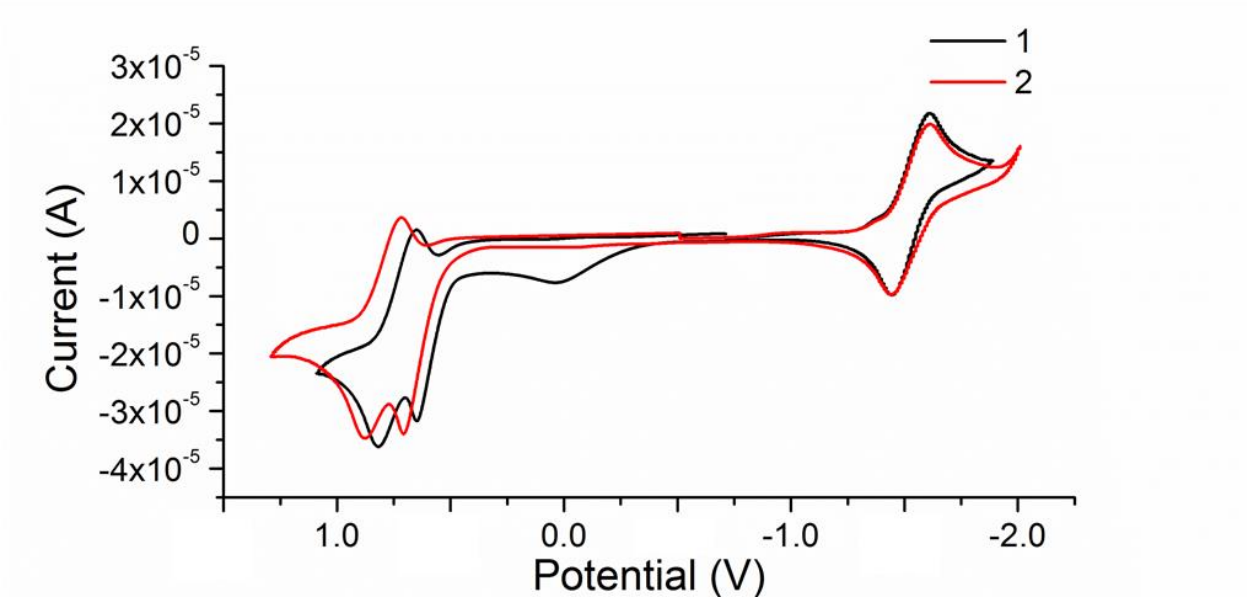

Figure S9. Cyclic voltammograms of complexes **1** and **2** in 0.1 M N(n-Bu)$_4$PF$_6$ solution in CH_2Cl_2 (potential vs. ferrocene/ferrocenium, scan rate: 100 mV/s).

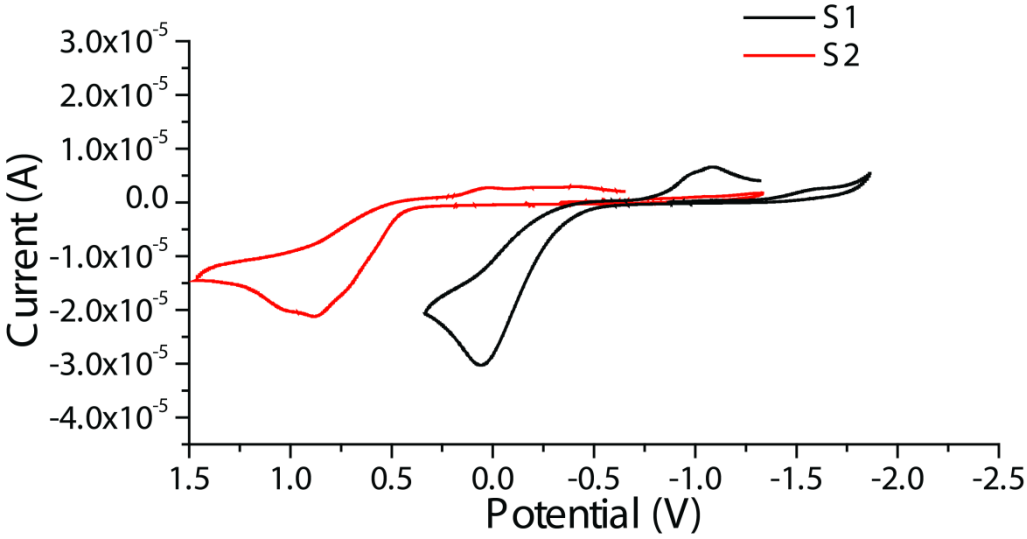

Figure S10. Cyclic voltammograms of model complexes **S1** and **S2** in 0.1 M N(n-Bu)$_4$PF$_6$ solution in CH_2Cl_2 (potential vs. ferrocene/ferrocenium, scan rate: 100 mV/s).

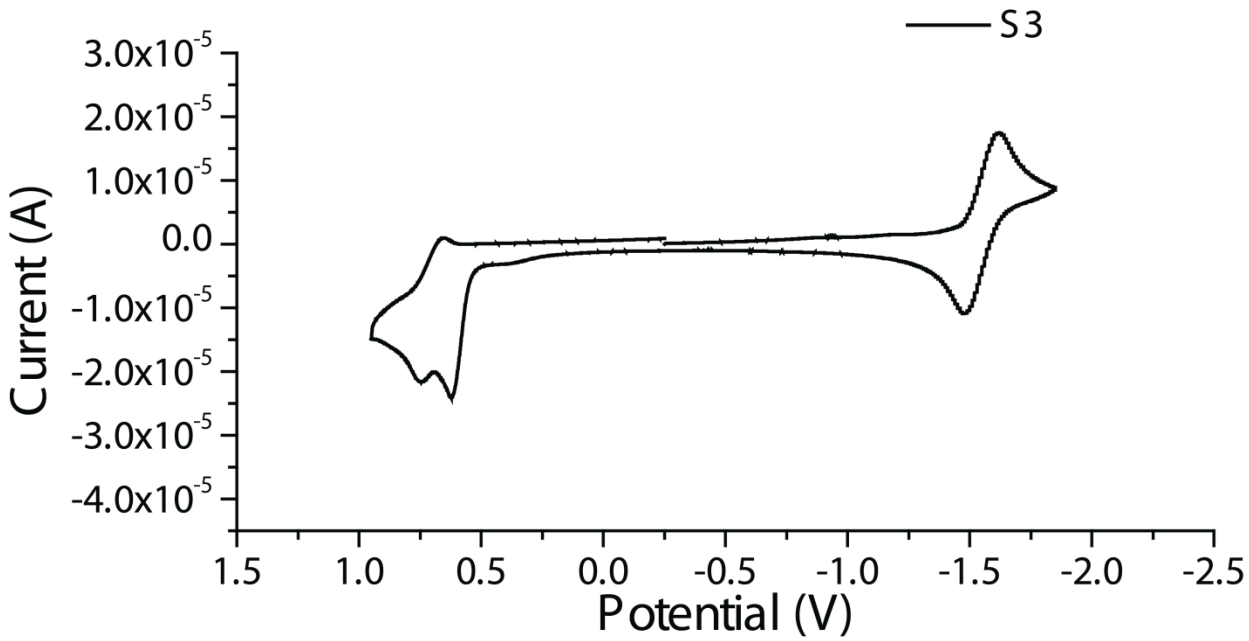

Figure S11. Cyclic voltammogram of Bodipy ligand **S3** in 0.1 M $N(n\text{-}Bu)_4PF_6$ solution in CH_2Cl_2 (potential vs. ferrocene/ferrocenium, scan rate: 100 mV/s).

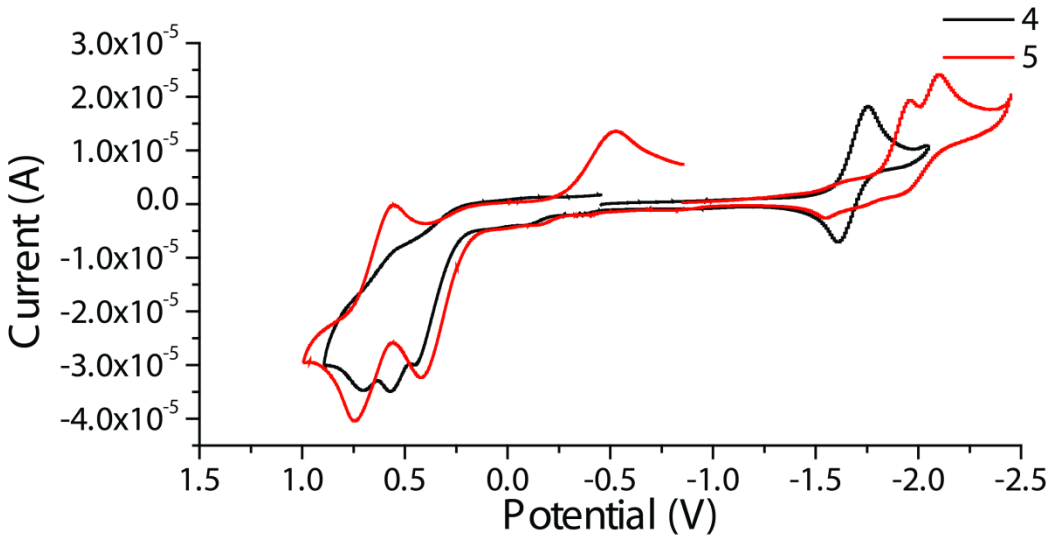

Figure S12. Cyclic voltammograms of complexes **4** and **5** in 0.1 M $N(n\text{-}Bu)_4PF_6$ solution in CH_2Cl_2 (potential vs. ferrocene/ferrocenium, scan rate: 100 mV/s).

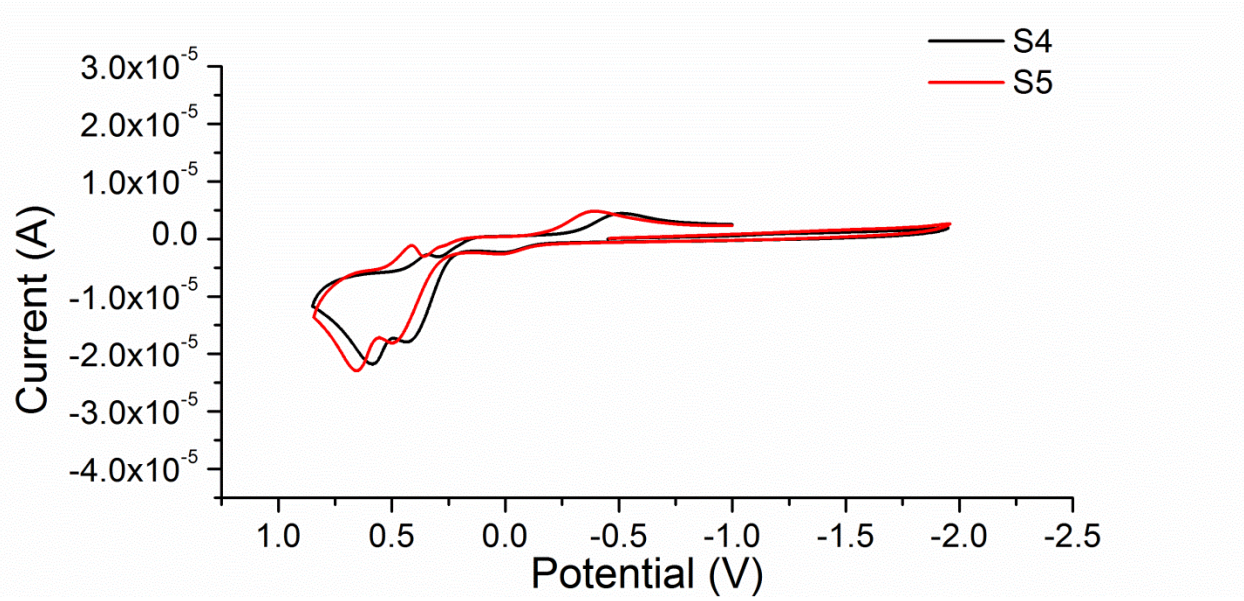

Figure S13. Cyclic voltammograms of model complexes **S4** and **S5** in 0.1 M $N(n\text{-}Bu)_4PF_6$ solution in CH_2Cl_2 (potential vs. ferrocene/ferrocenium, scan rate: 100 mV/s).

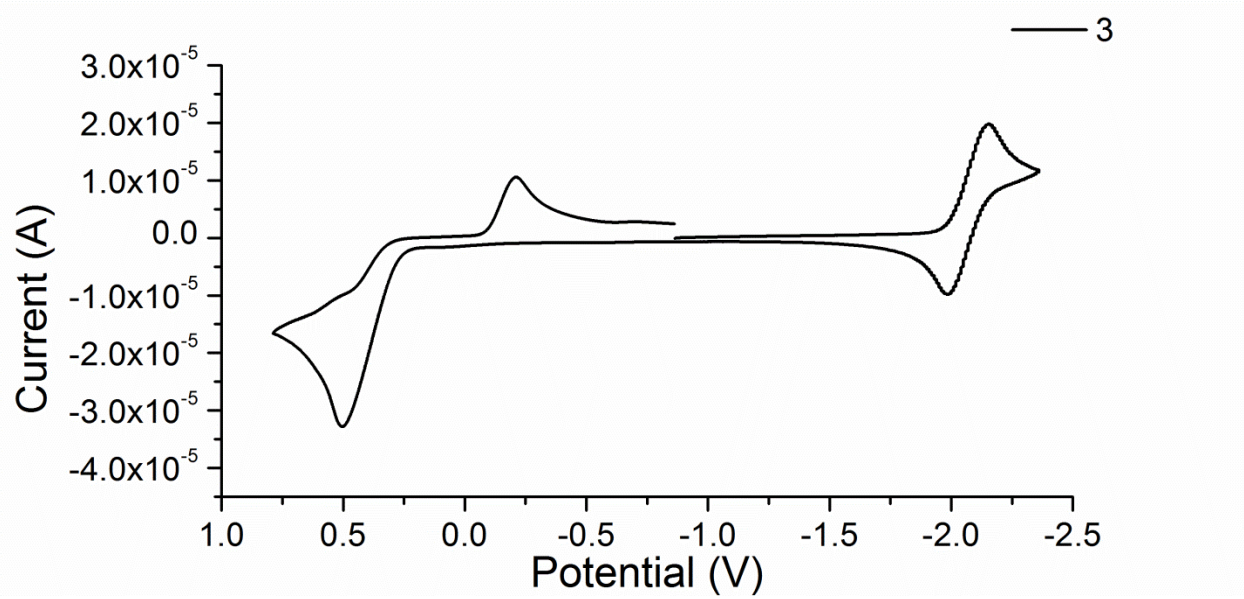

Figure S14. Cyclic voltammogram of ligand **3** in 0.1 M $N(n\text{-}Bu)_4PF_6$ solution in CH_2Cl_2 (potential vs. ferrocene/ferrocenium, scan rate: 100 mV/s).

Spectroelectrochemistry

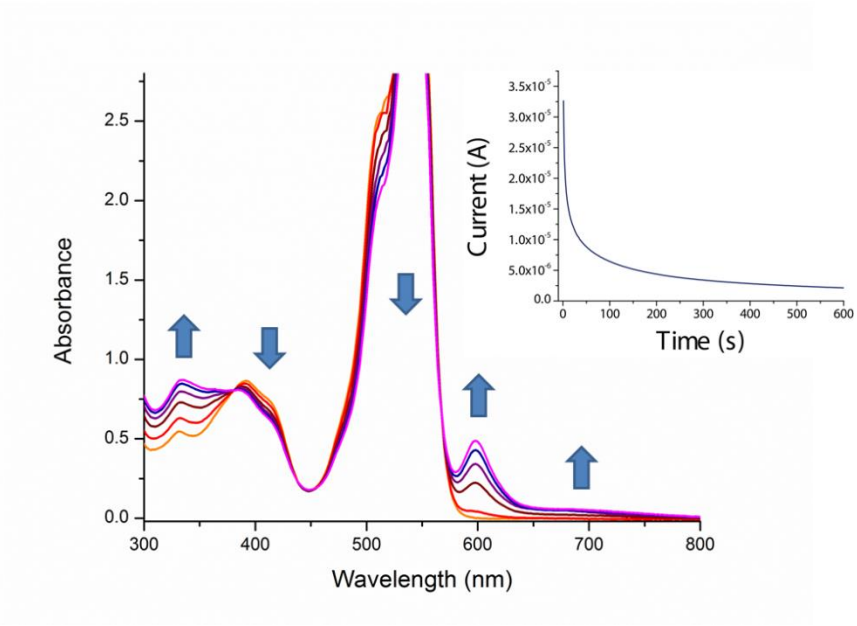

Figure S15. Spectral changes observed upon controlled-potential, bulk electrolysis of Bodipy ligand **S3** at -1600 mV in a 0.1 M $N(n\text{-}Bu)_4PF_6$ solution in CH_2Cl_2. Inset: current vs. time profile throughout electrolysis.

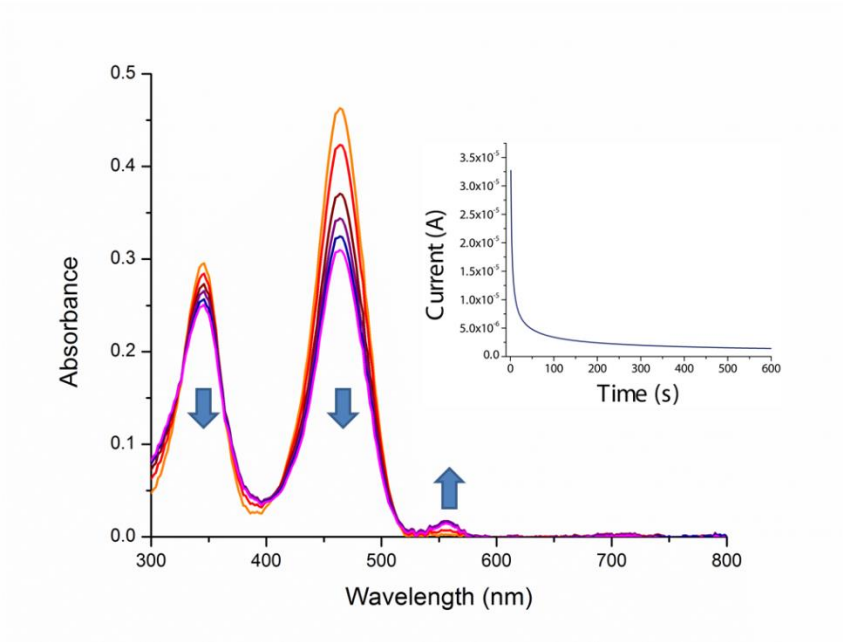

Figure S16. Spectral changes observed upon controlled-potential, bulk electrolysis of Bodipy ligand **3** at -2100 mV in a 0.1 M $N(n\text{-}Bu)_4PF_6$ solution in CH_2Cl_2. Inset: current vs. time profile throughout electrolysis.

Transient Absorption Spectroscopy

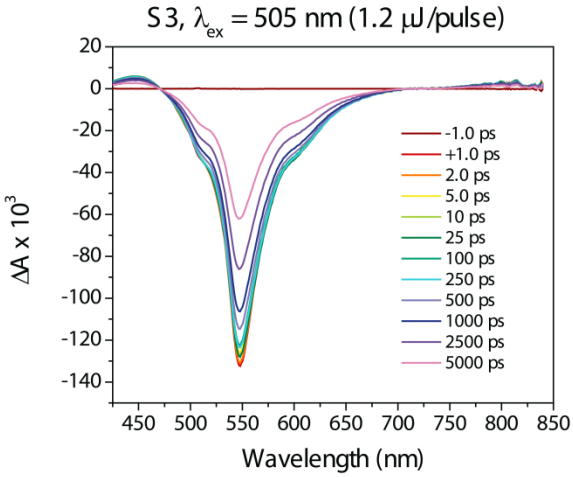

Figure S17. Transient absorption spectra of ligand **S3** in CH_2Cl_2.

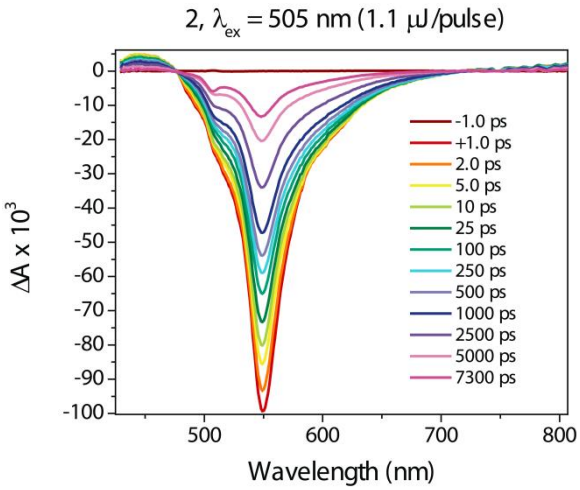

Figure S18. Transient absorption spectra of complex **2** in CH_2Cl_2.

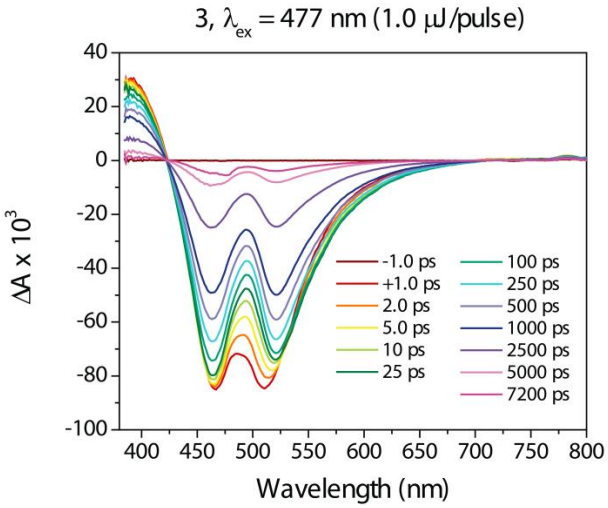

Figure S19. Transient absorption spectra of Bodipy ligand **3** in CH_2Cl_2.

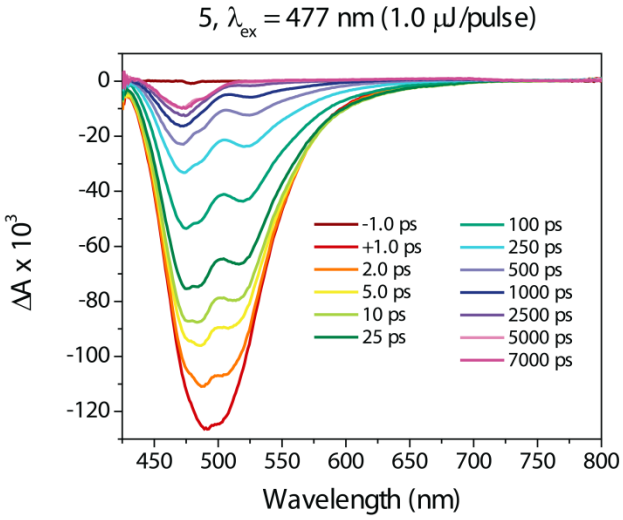

Figure S20. Transient absorption spectra of complex **5** in CH_2Cl_2.

Computational

DFT calculations were made using the Amsterdam Density Functional (ADF2013.01) suite on a 16-core Parallel Quantum Solutions (PQS) computational cluster. Geometry optimizations were made without restraint in the ADF GUI using basis sets containing triple-ζ functions with two polarization function (TZ2P), and the local density approximations of Becke[5] and Perdew.[6] This was followed by single point calculations using triple-ζ functions with two polarization functions (TZ2P) and the PBE-hybrid (PBE0) functional by Ernzerhof-Scuseria[5] and by Adamo-Barone.[6] Kohn-Sham representations of frontier orbitals were generated by the ADF 2013.01 GUI. Electron density plots with electron density potential mapped onto them for complexes **1** and **2** in their solid state conformations were calculated at the PBE-hybrid (PBE0) level of theory and mapped with the 0.03 $e^-/Å^3$ isodensity value.

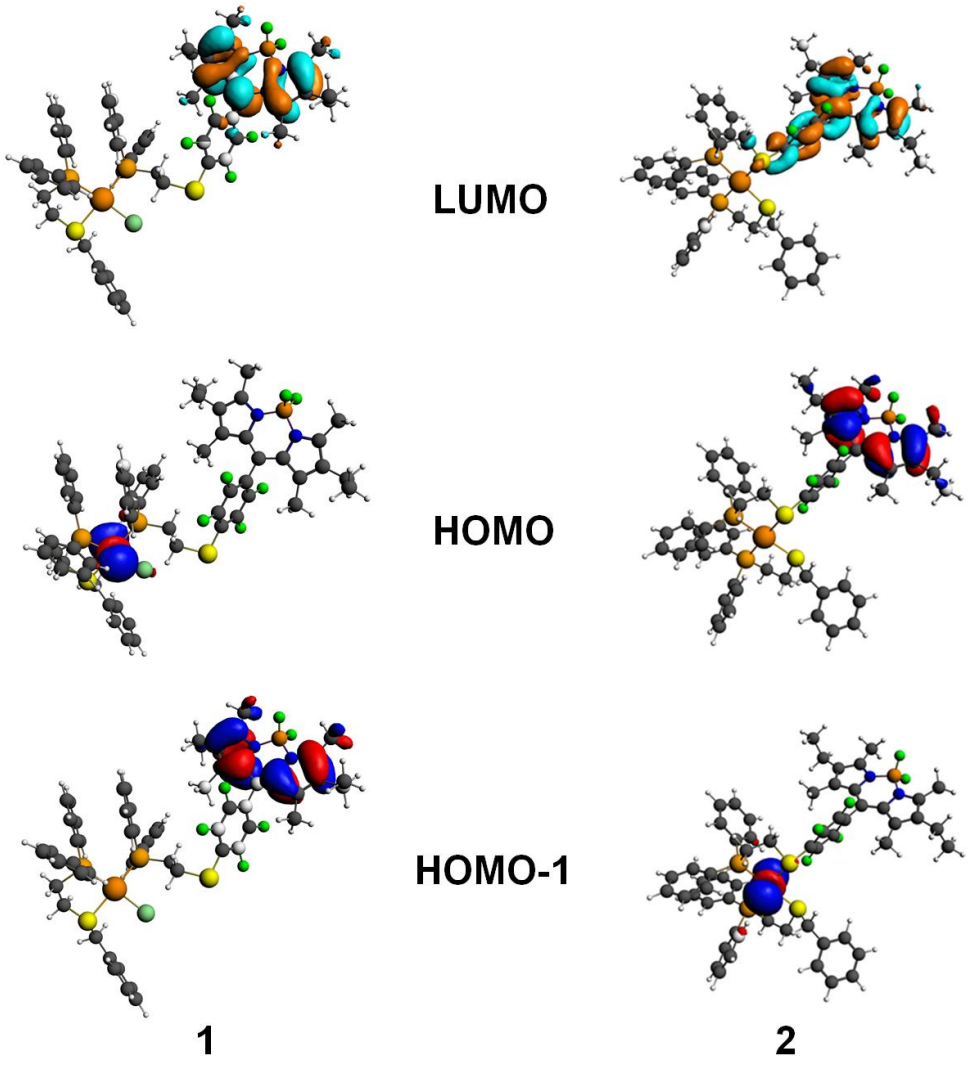

Figure S21. Modeling of HOMO-1, HOMO and LUMO orbitals of complexes **1** and **2** determined via single point DFT calculations.

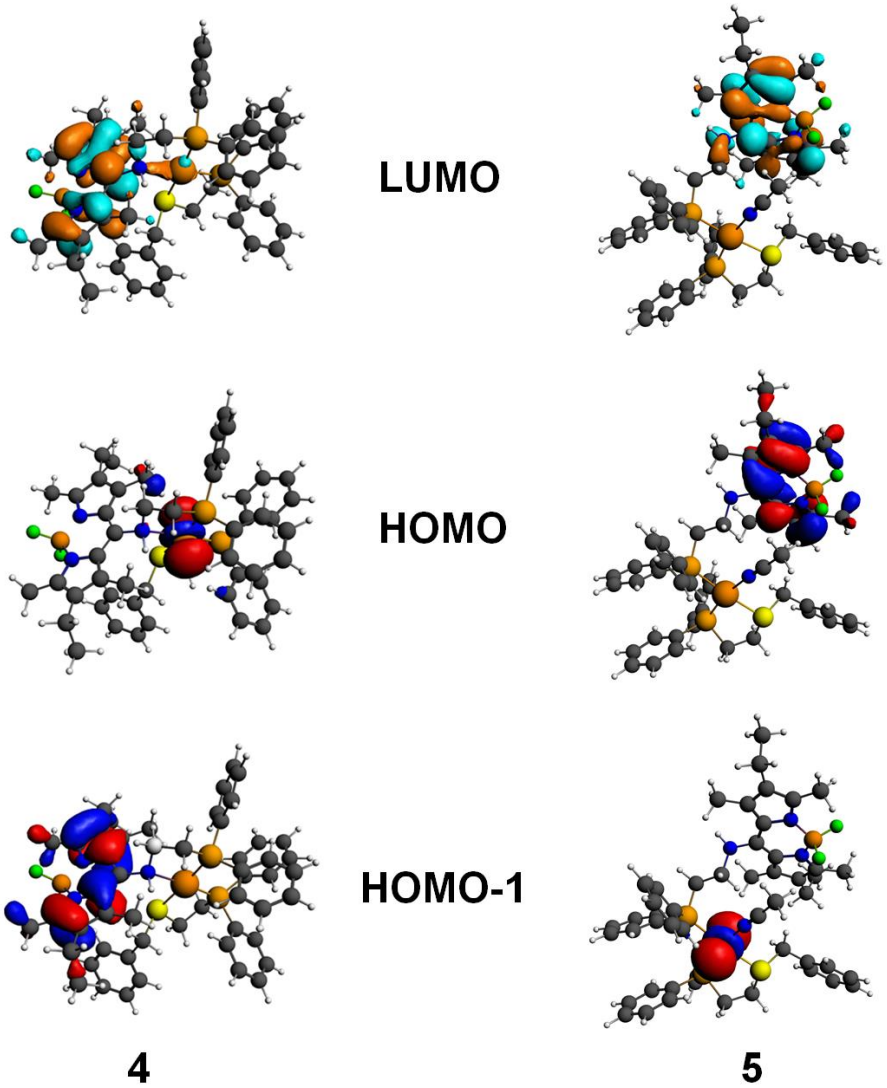

Figure S22. Modeling of HOMO-1, HOMO and LUMO orbitals of complexes **4** and **5** determined via single point DFT calculations.

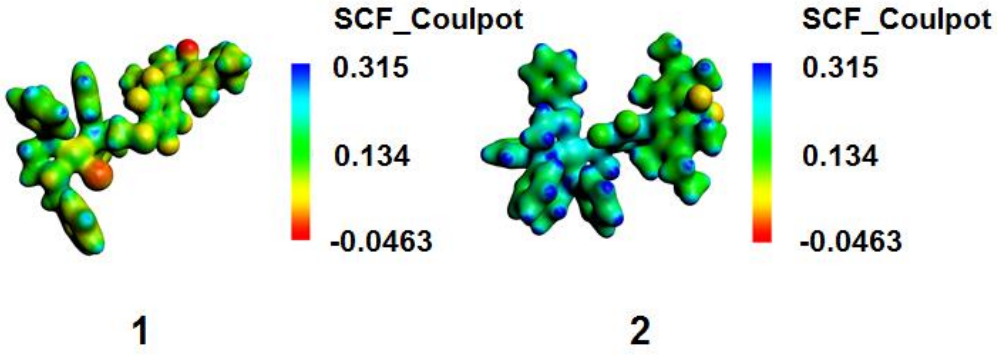

Figure S23. Electrostatic potential maps of complexes **1** and **2** depicting changes in electron density at the Rh(I) metal center upon changes in coordination sphere charge.

1, 1H NMR, CD_2Cl_2

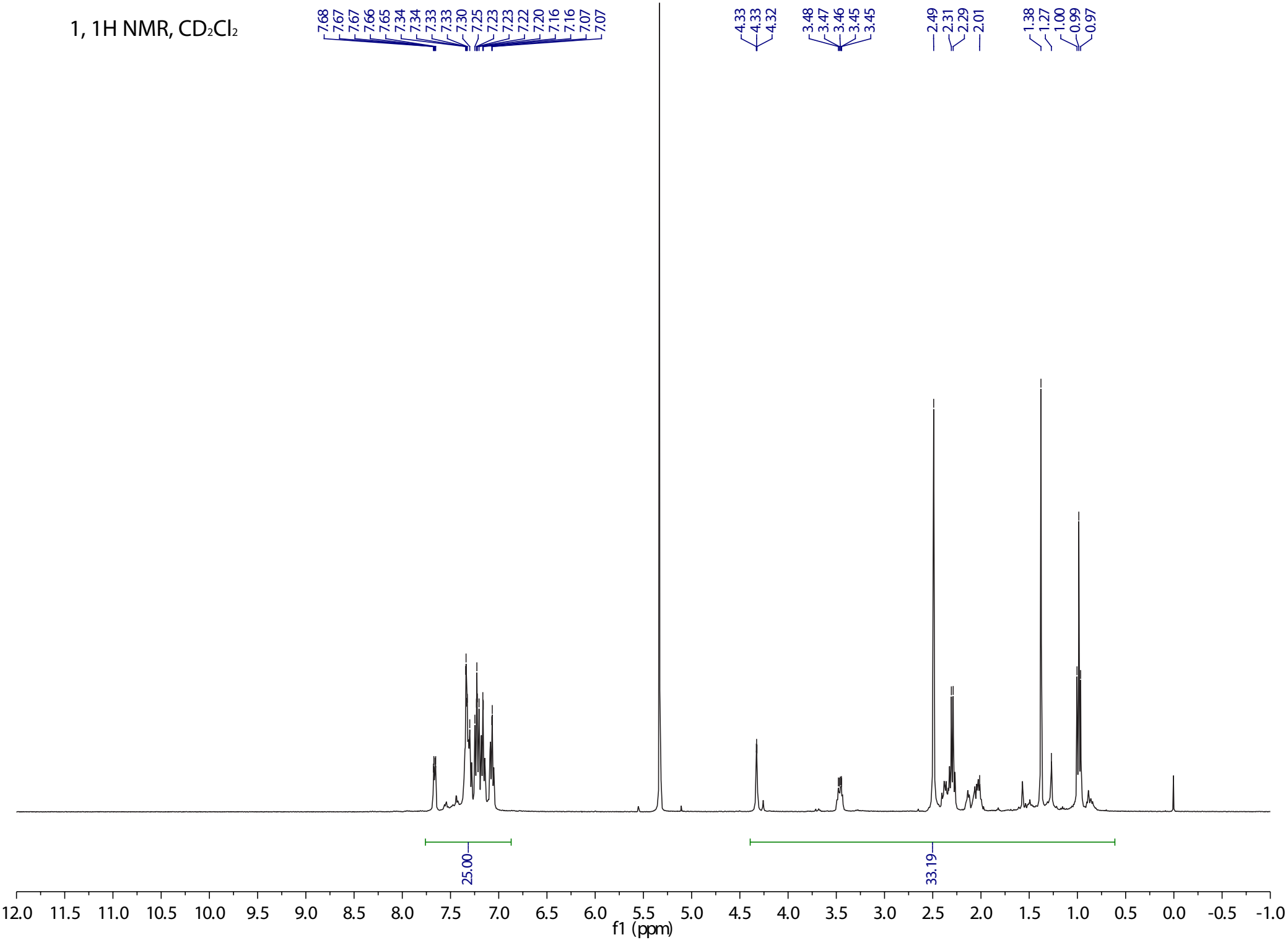

1, 31P{1H} NMR, CD_2Cl_2

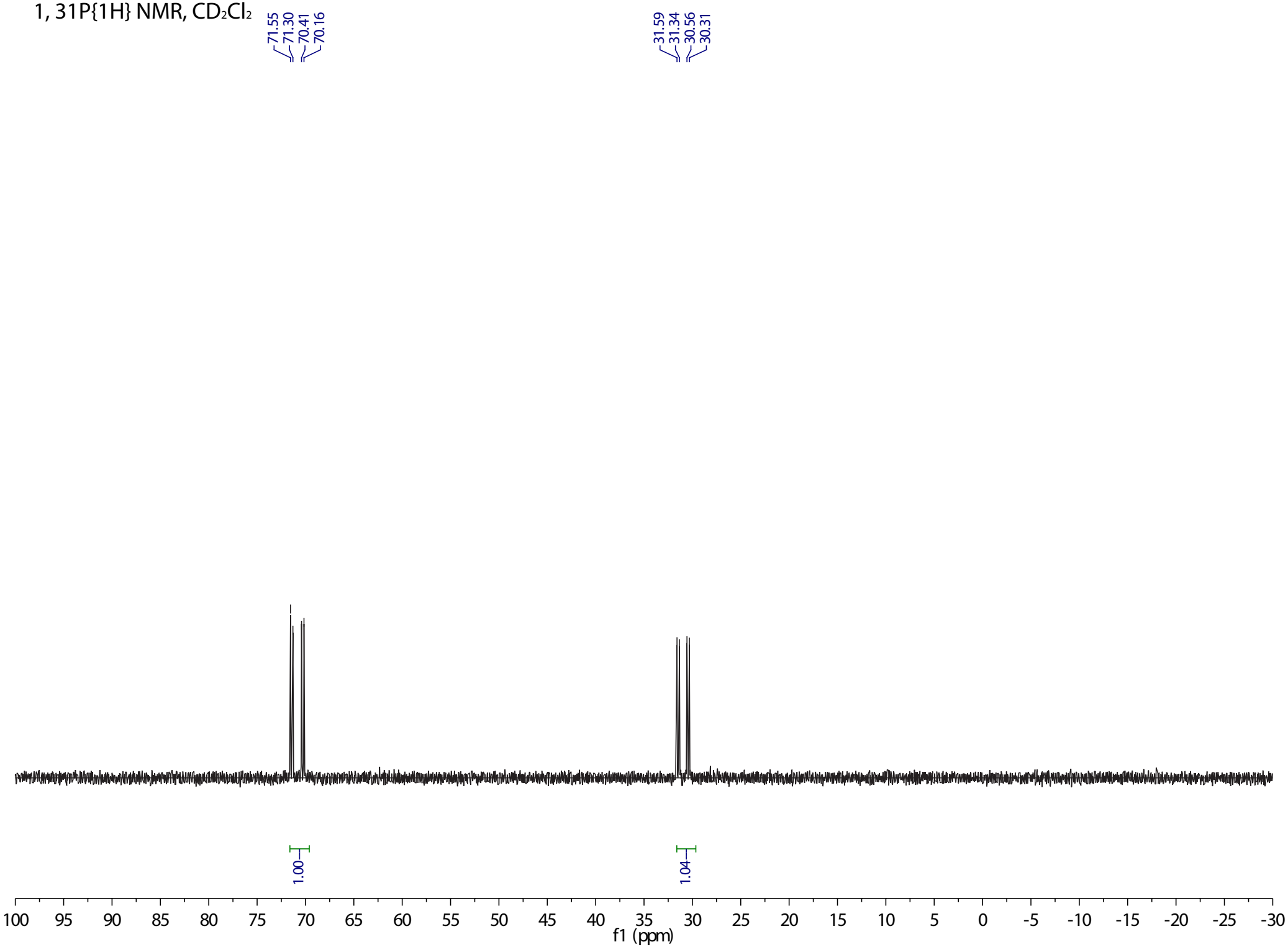

1, 19F NMR, CD_2Cl_2

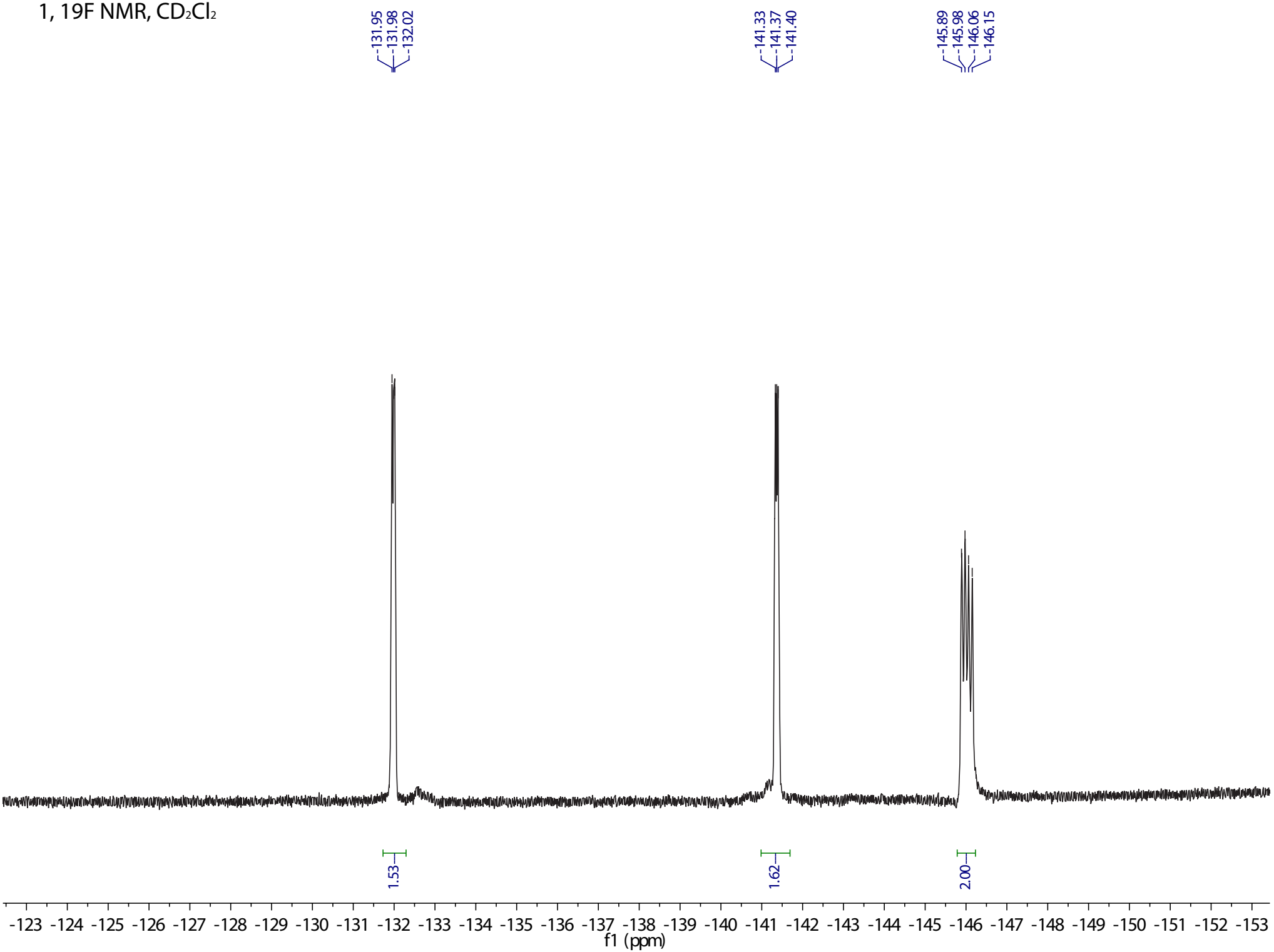

1, 11B{1H} NMR, CD_2Cl_2

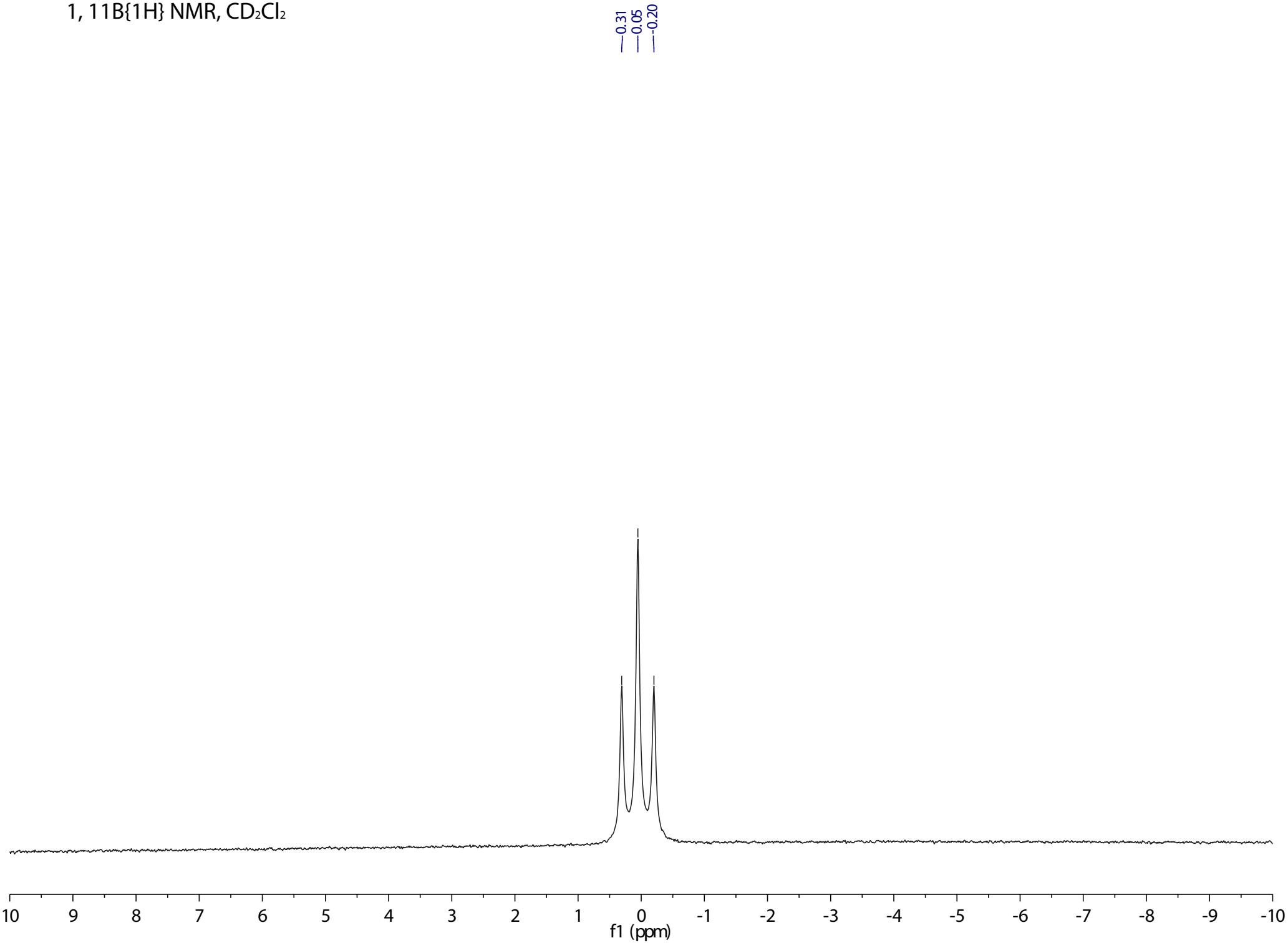

2, 1H NMR, CD_2Cl_2

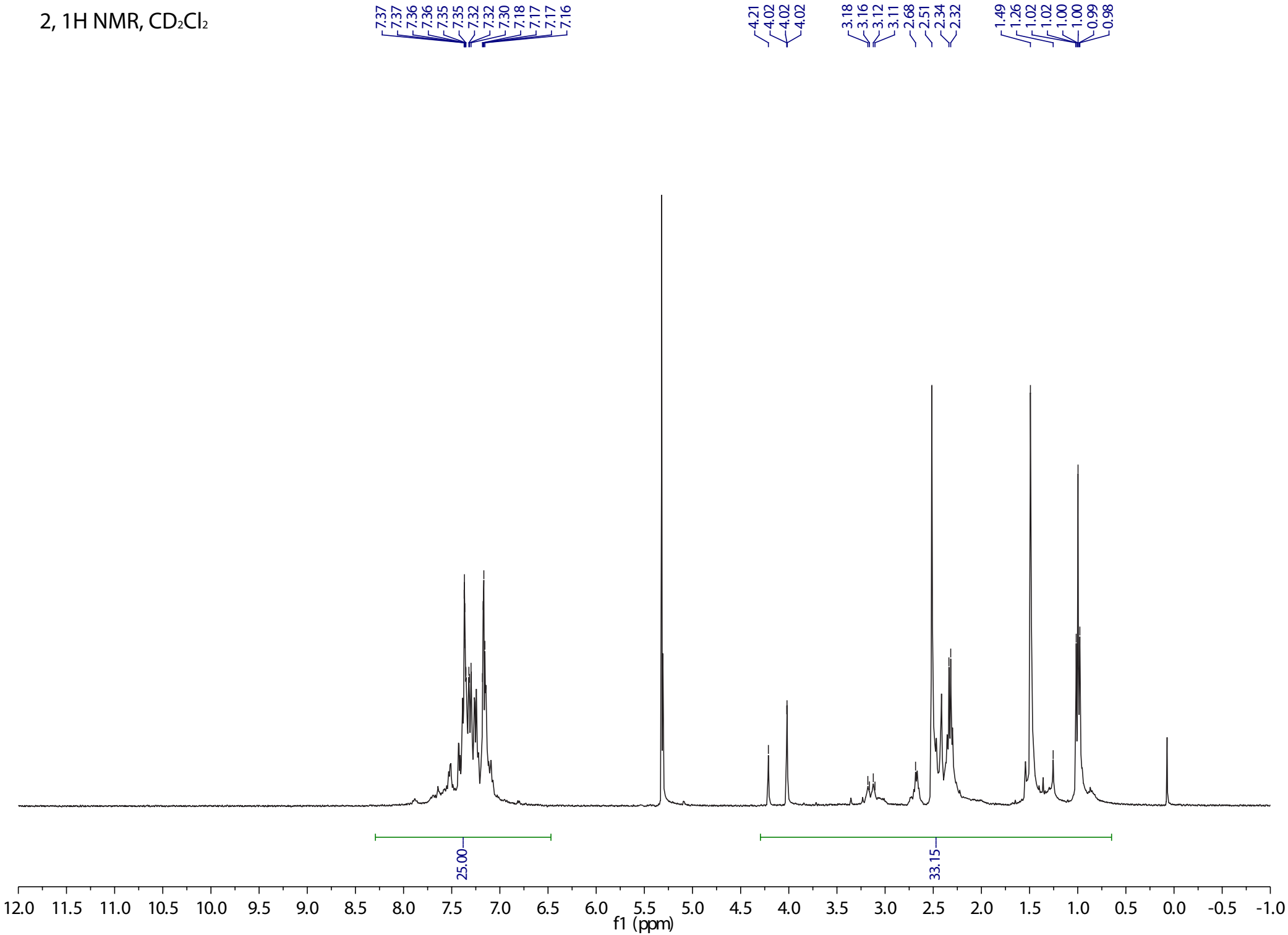

2, 31P{1H} NMR, CD_2Cl_2

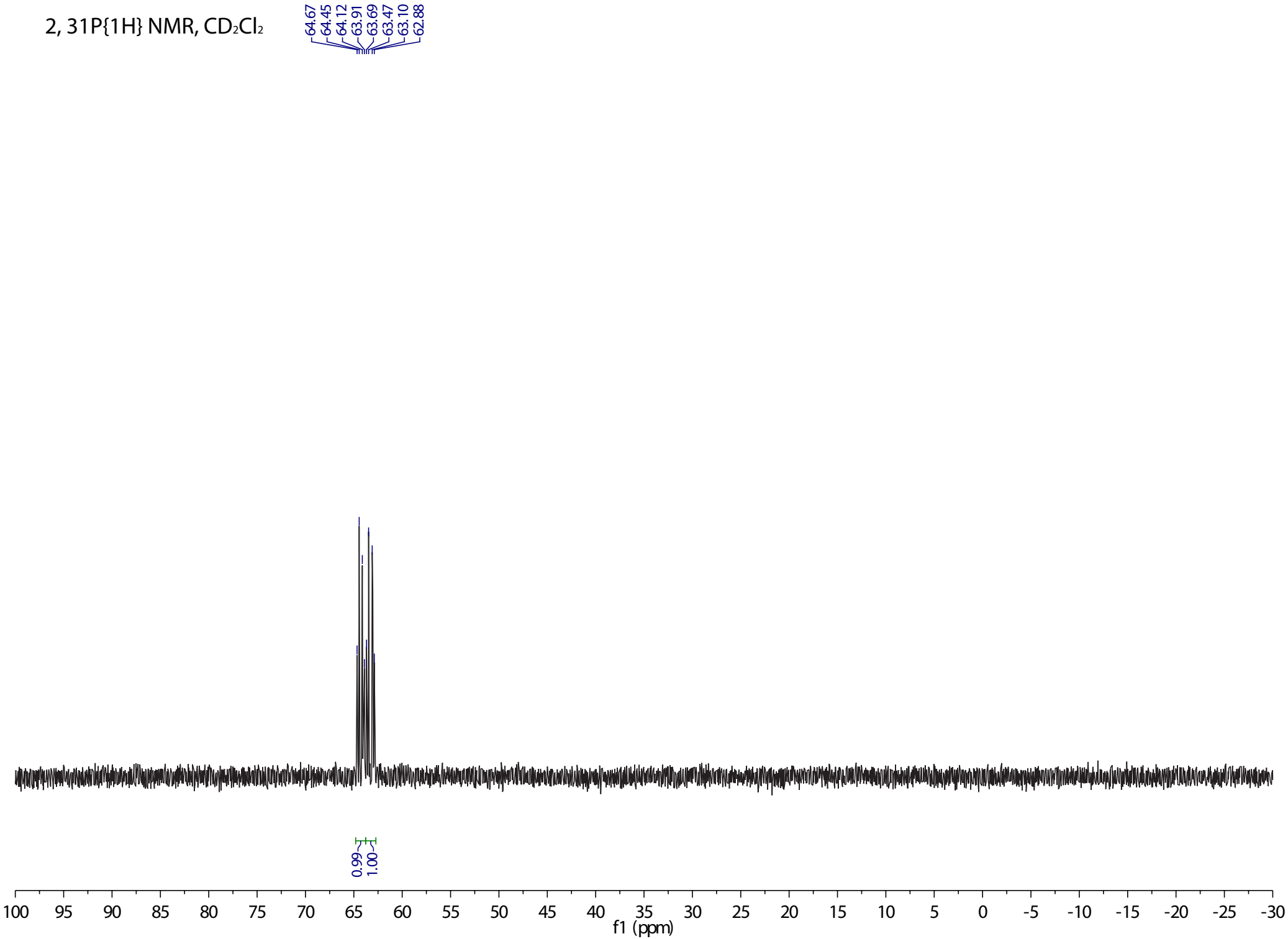

2, 19F NMR, CD_2Cl_2

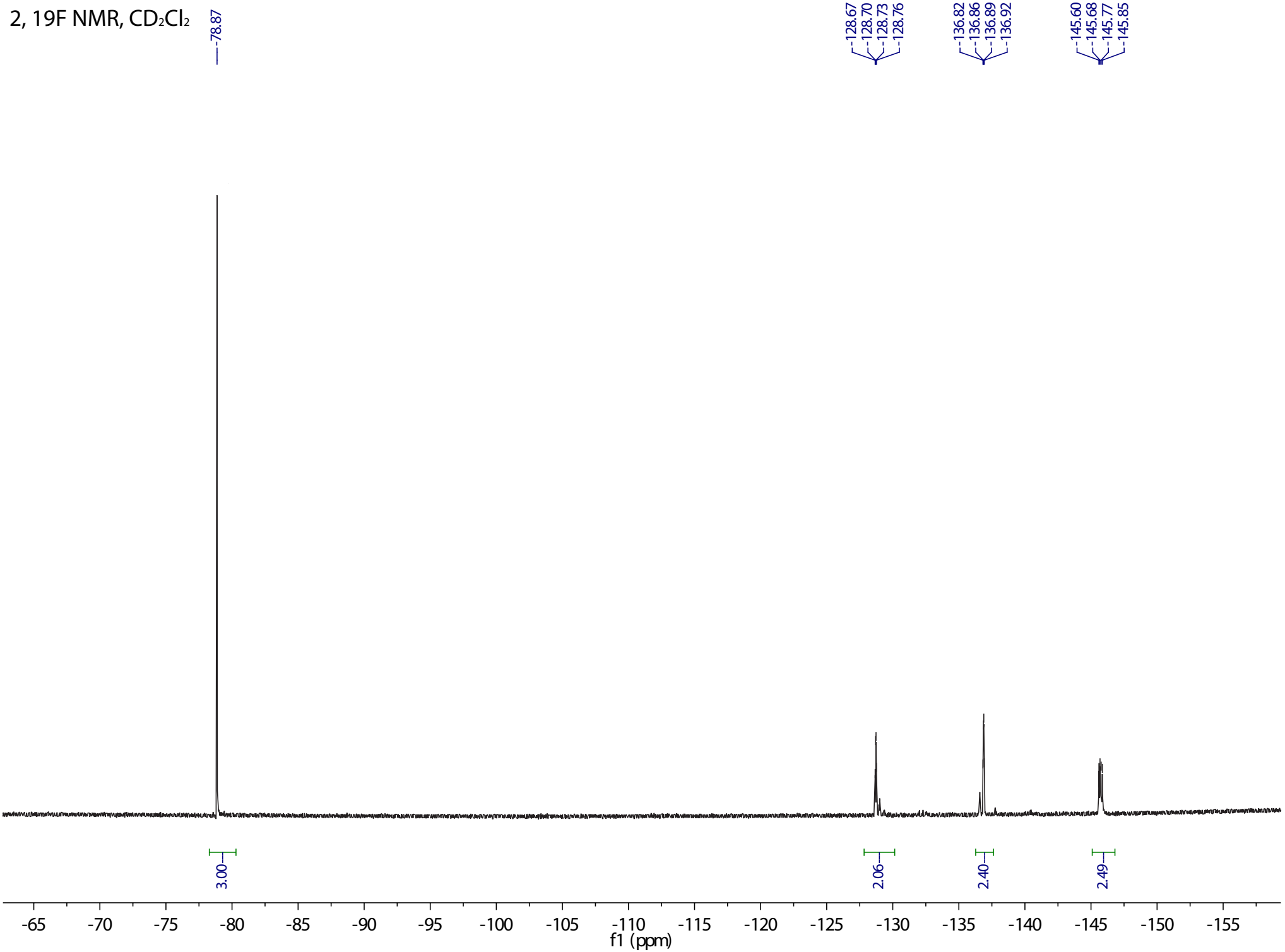

2, 11B{1H} NMR, CD_2Cl_2

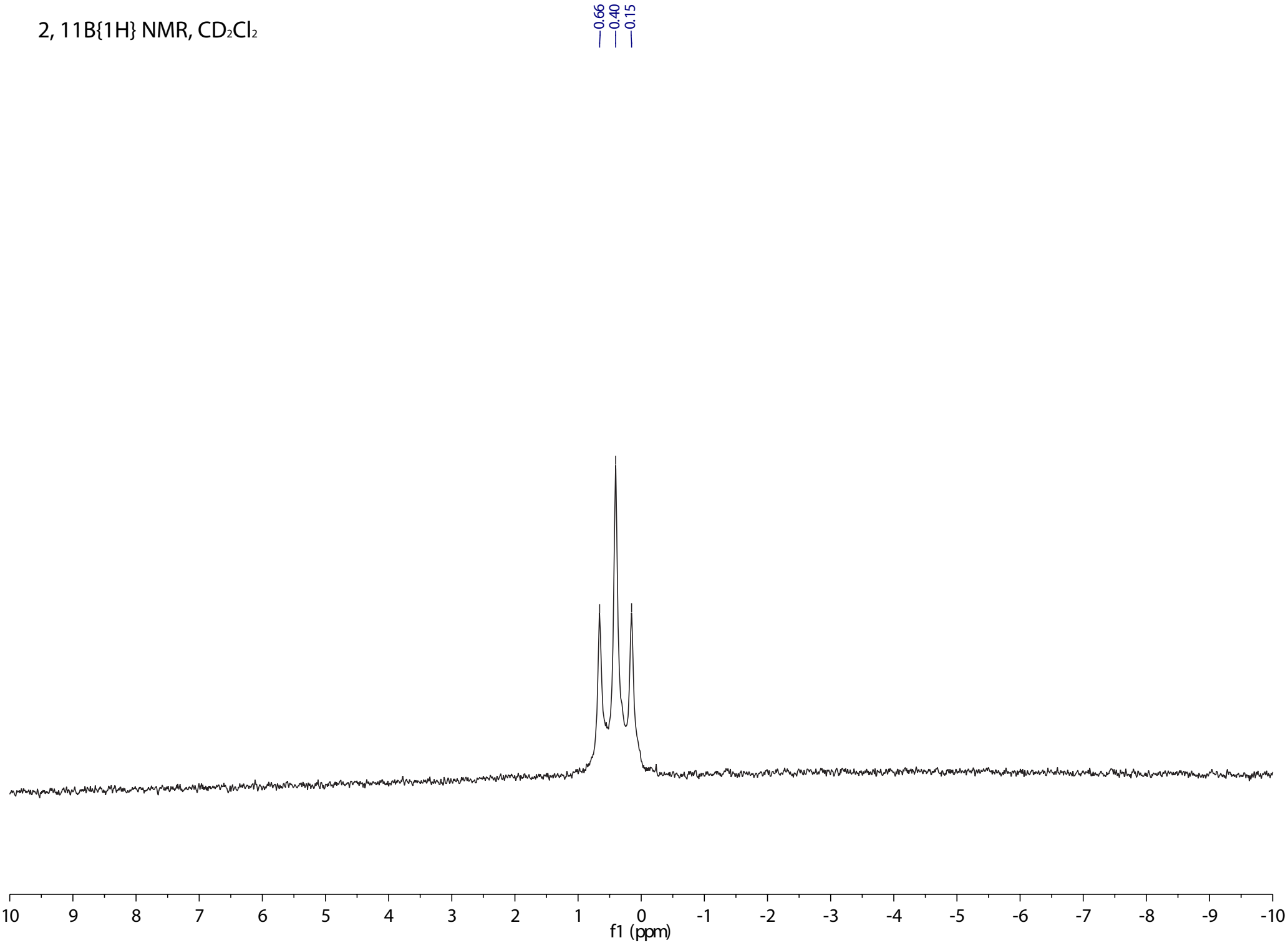

3, 1H NMR, CD2Cl2

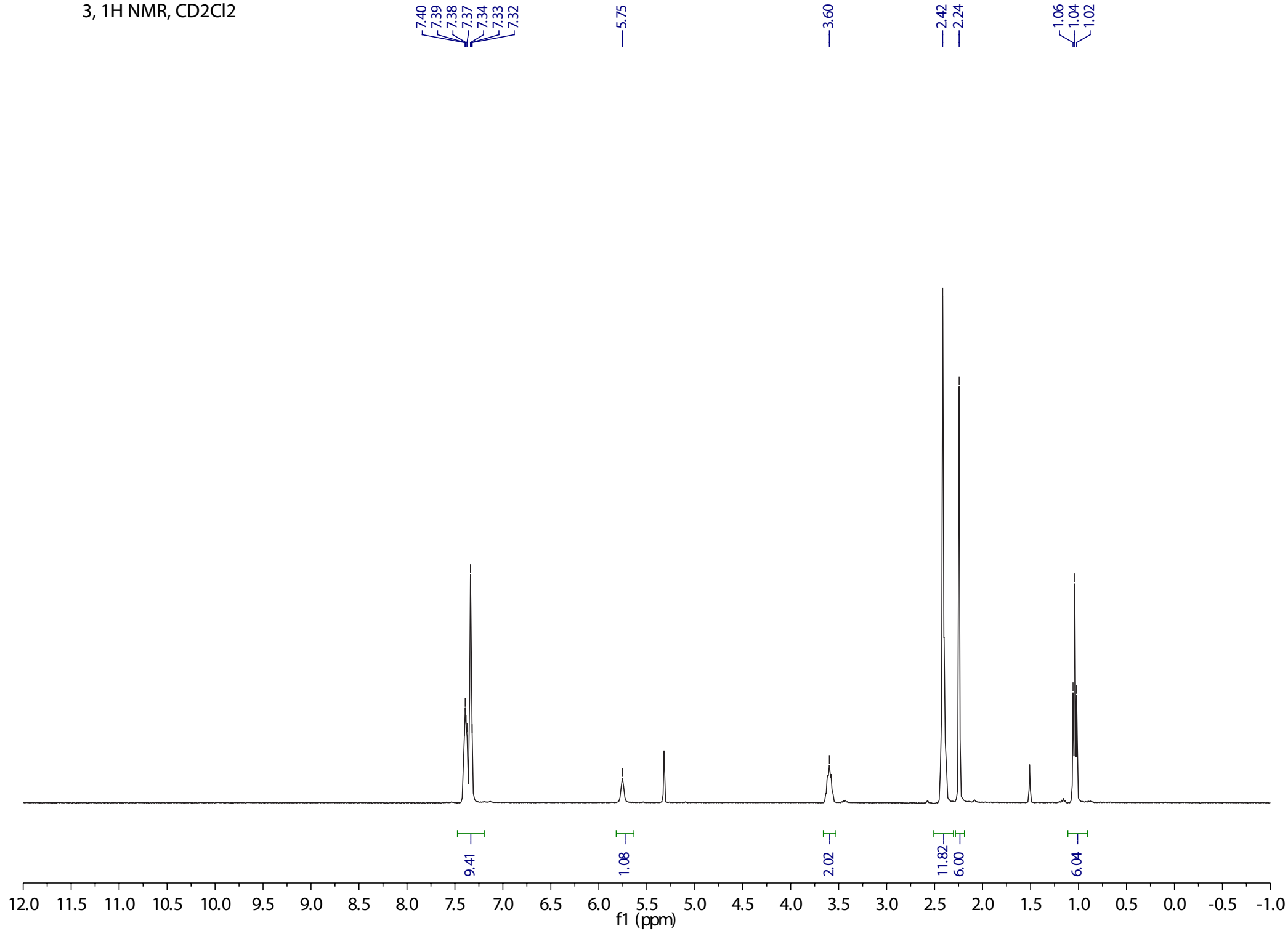

3, 13C{1H} NMR, CD_2Cl_2

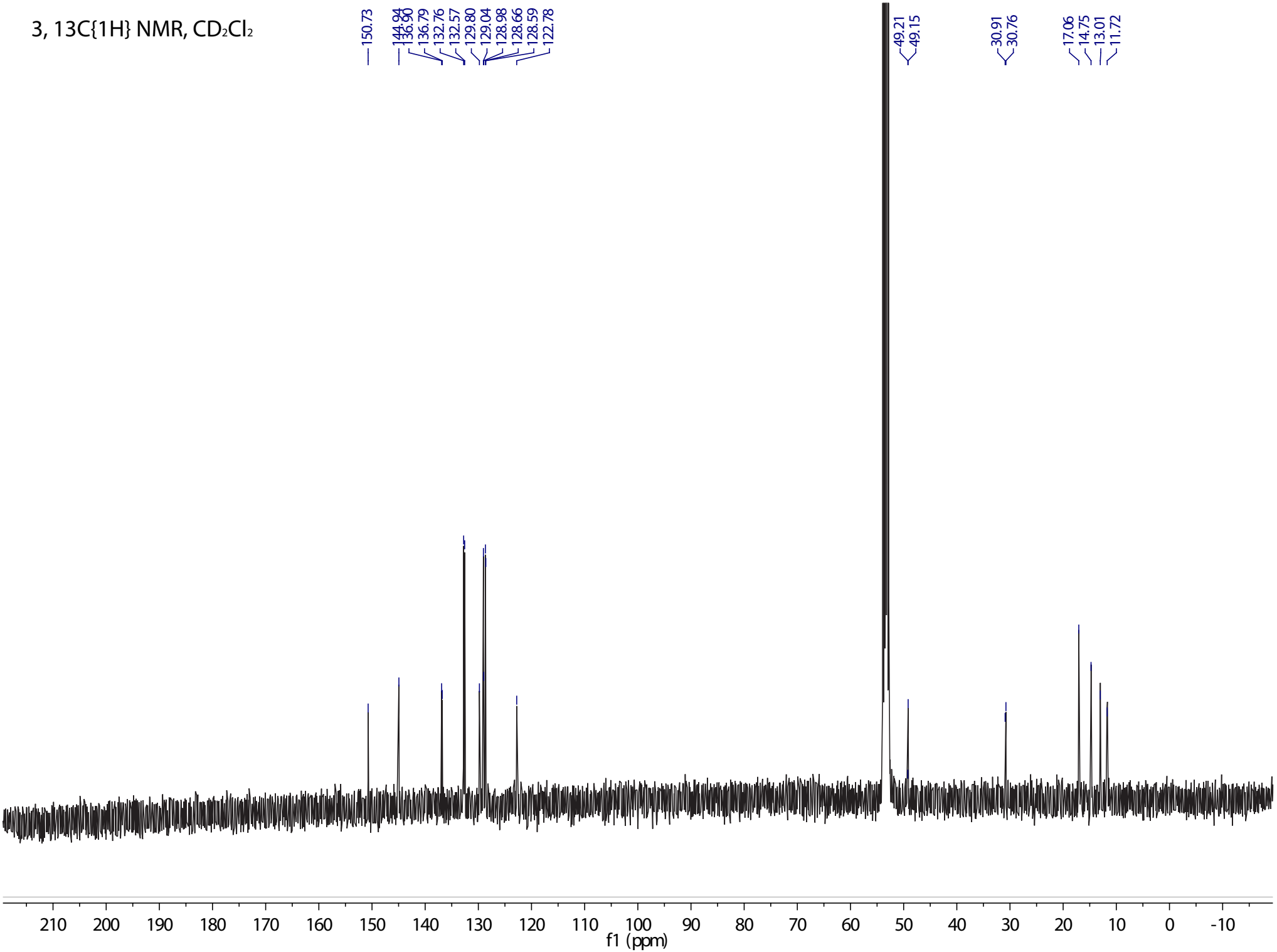

3, {1H}31P NMR, CD2Cl2

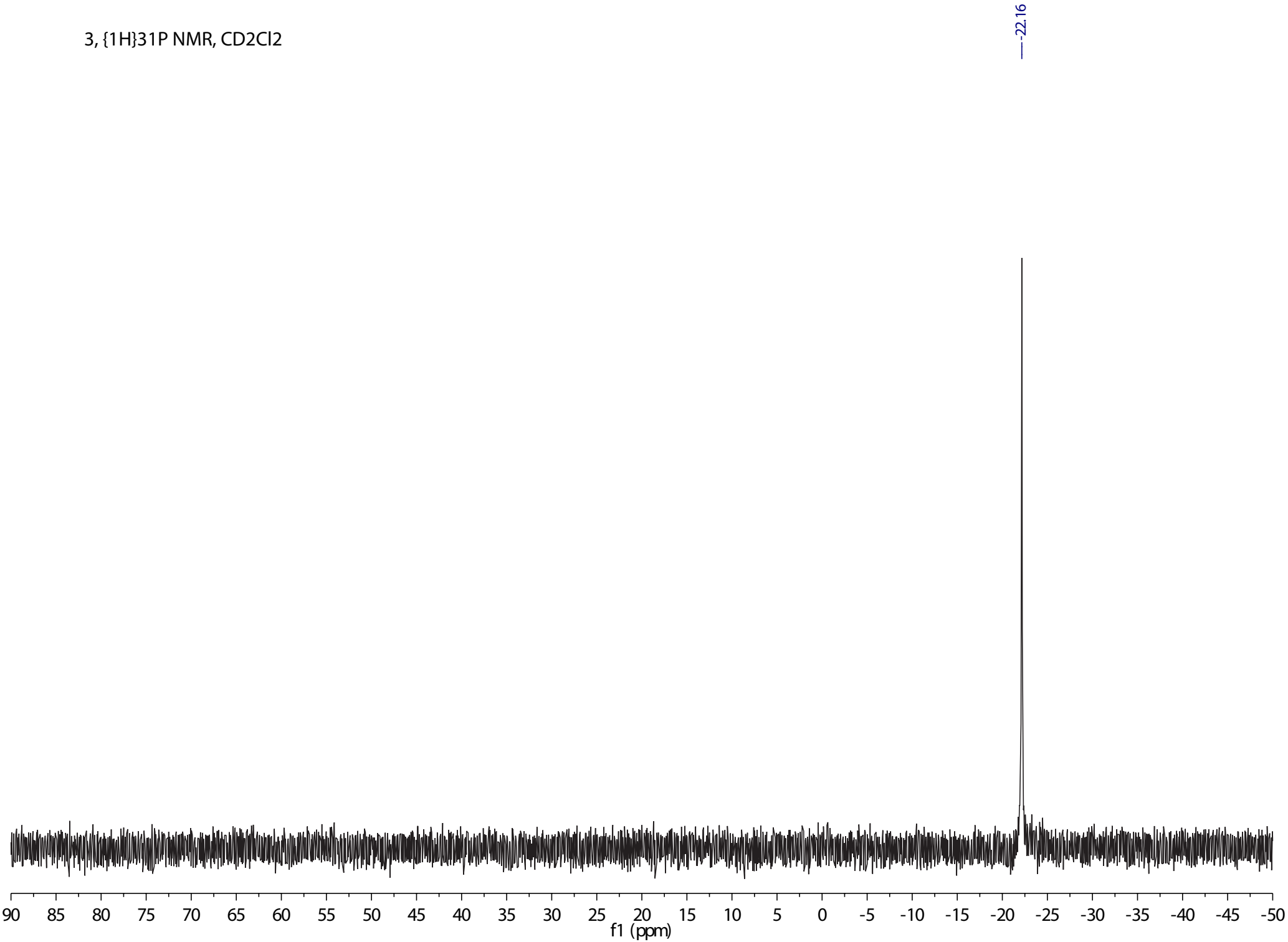

3, 19F NMR, CD2Cl2

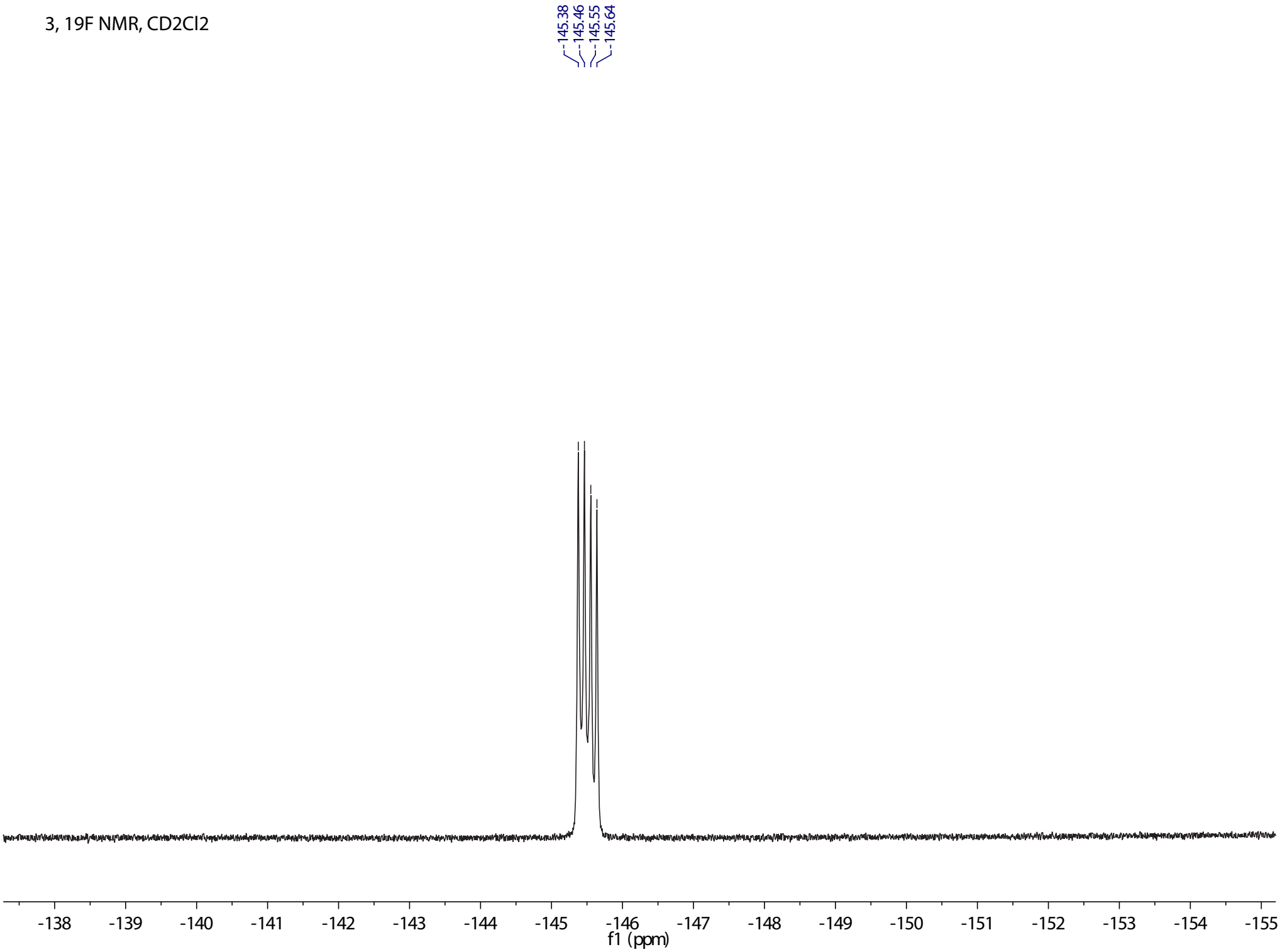

3, {1H}11B NMR, CD2Cl2

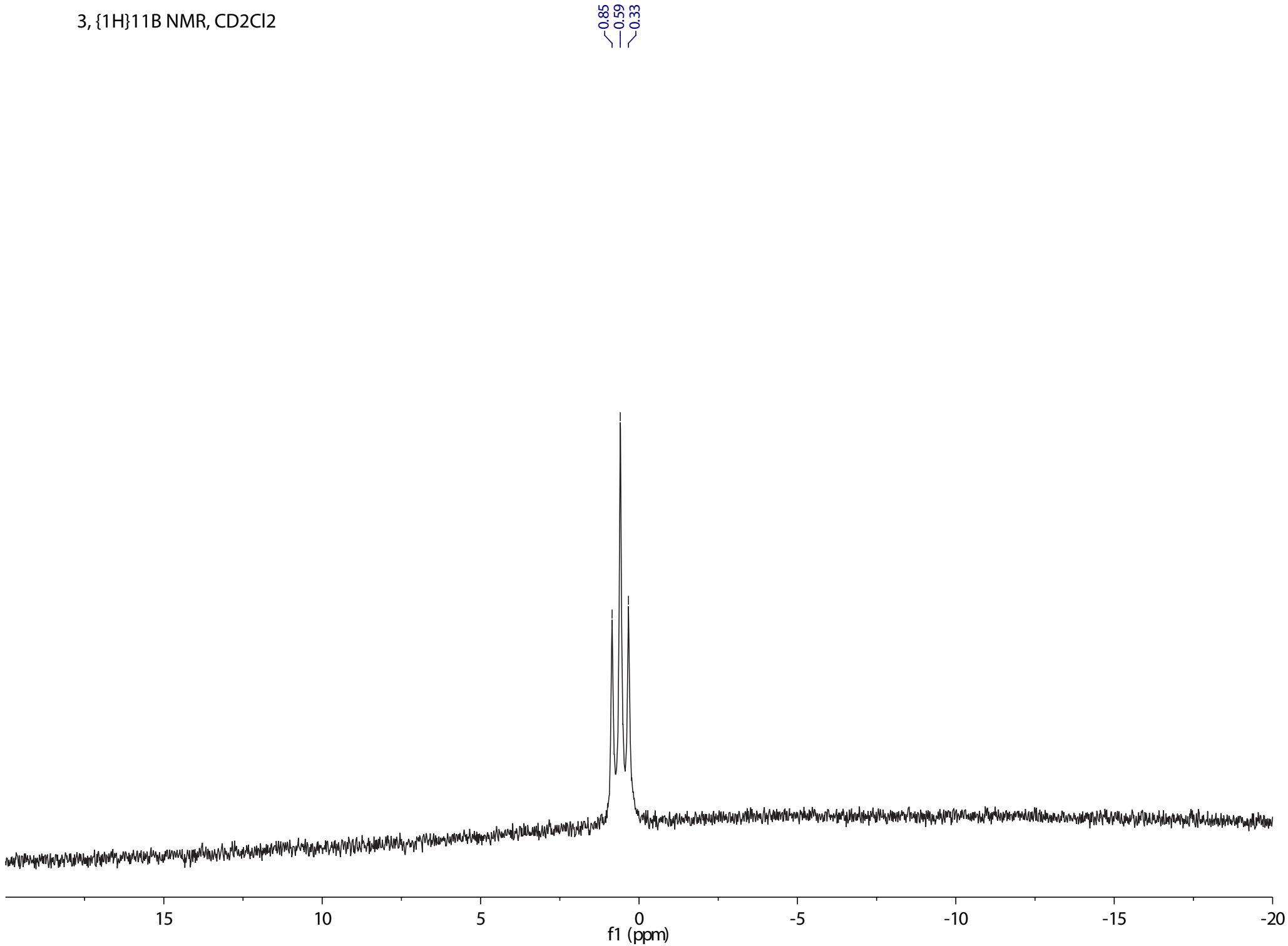

4, 1H NMR, CD_2Cl_2

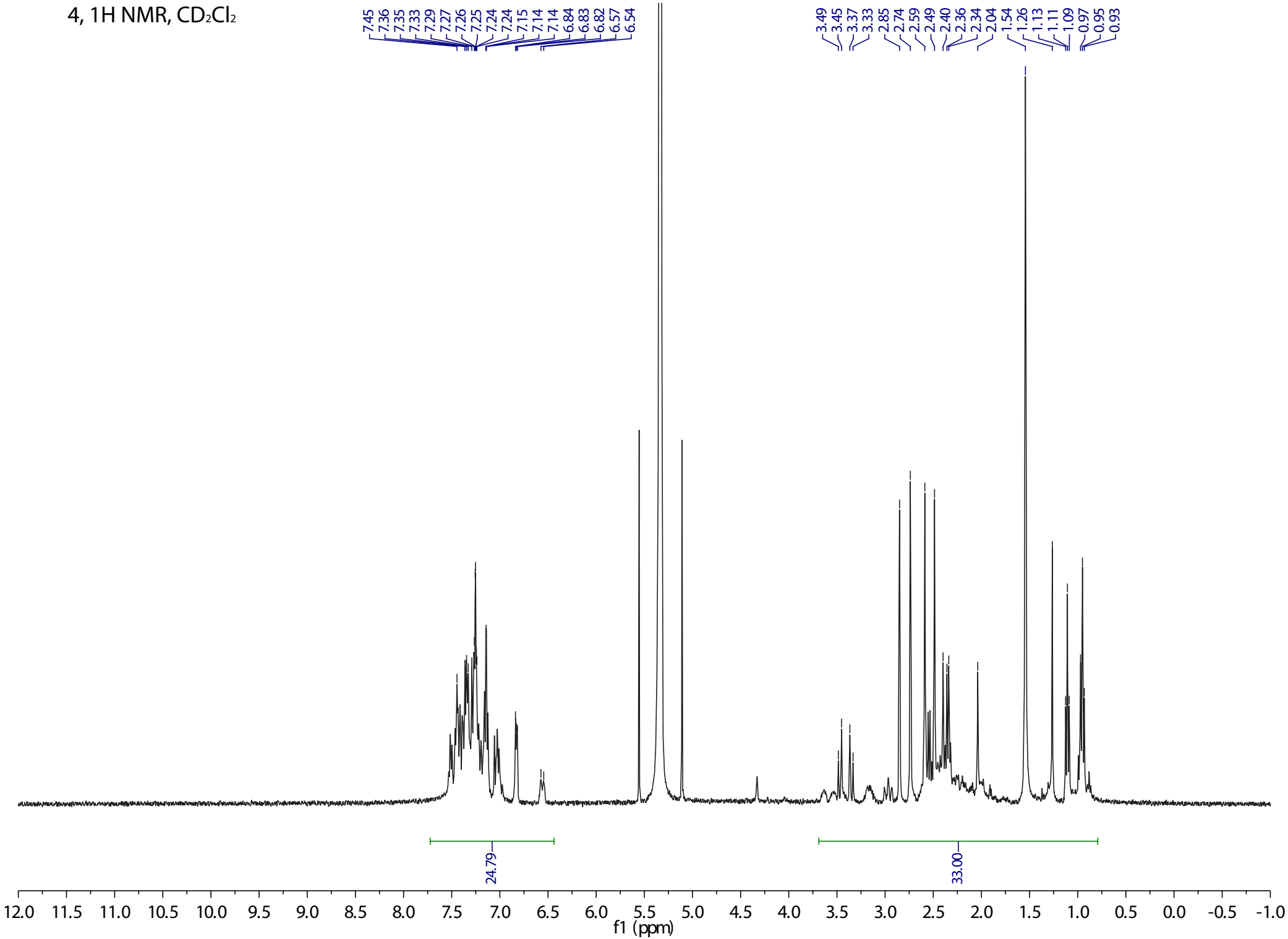

4, 31P{1H} NMR, CD_2Cl_2

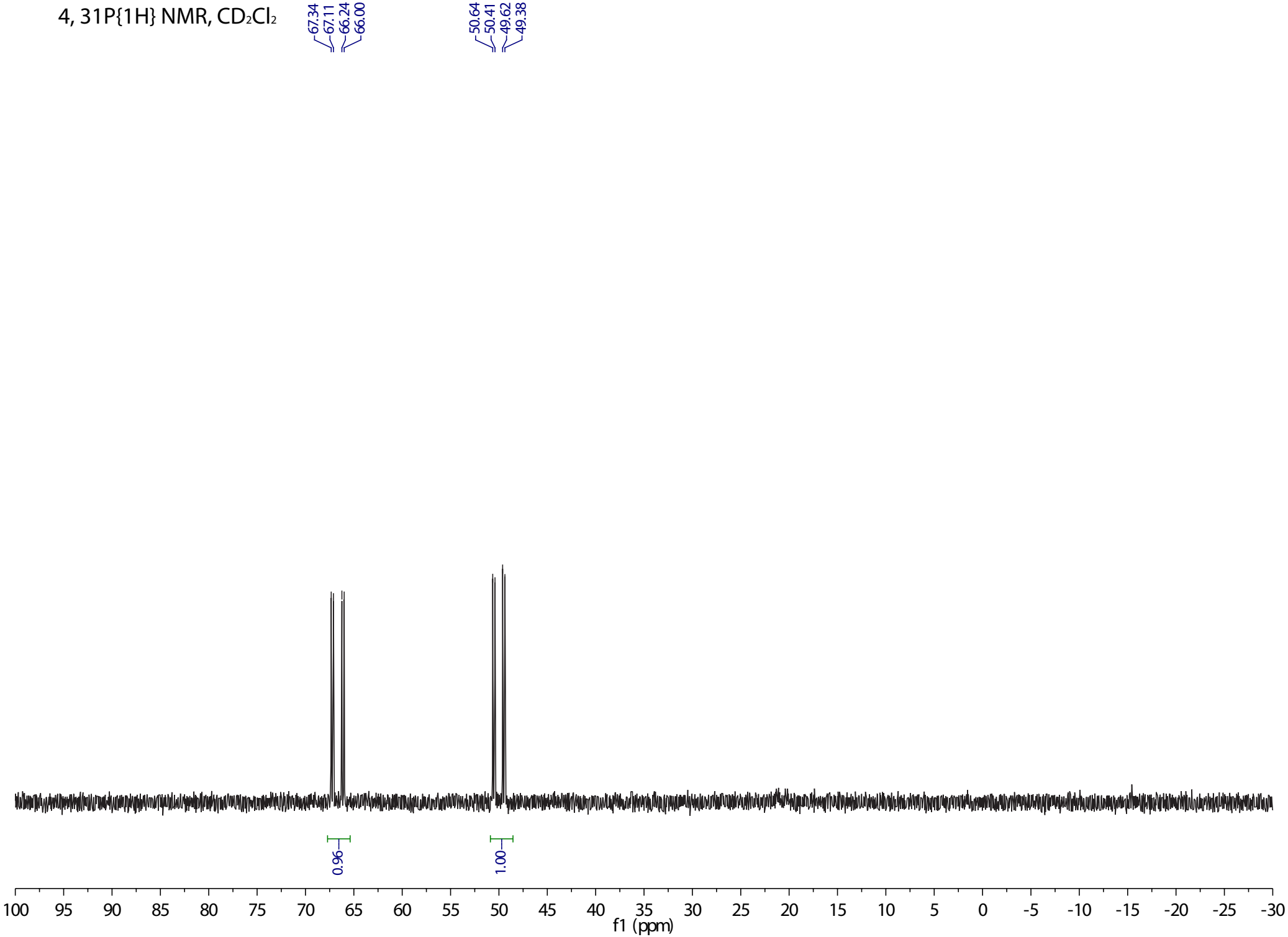

4, 19F NMR, CD_2Cl_2

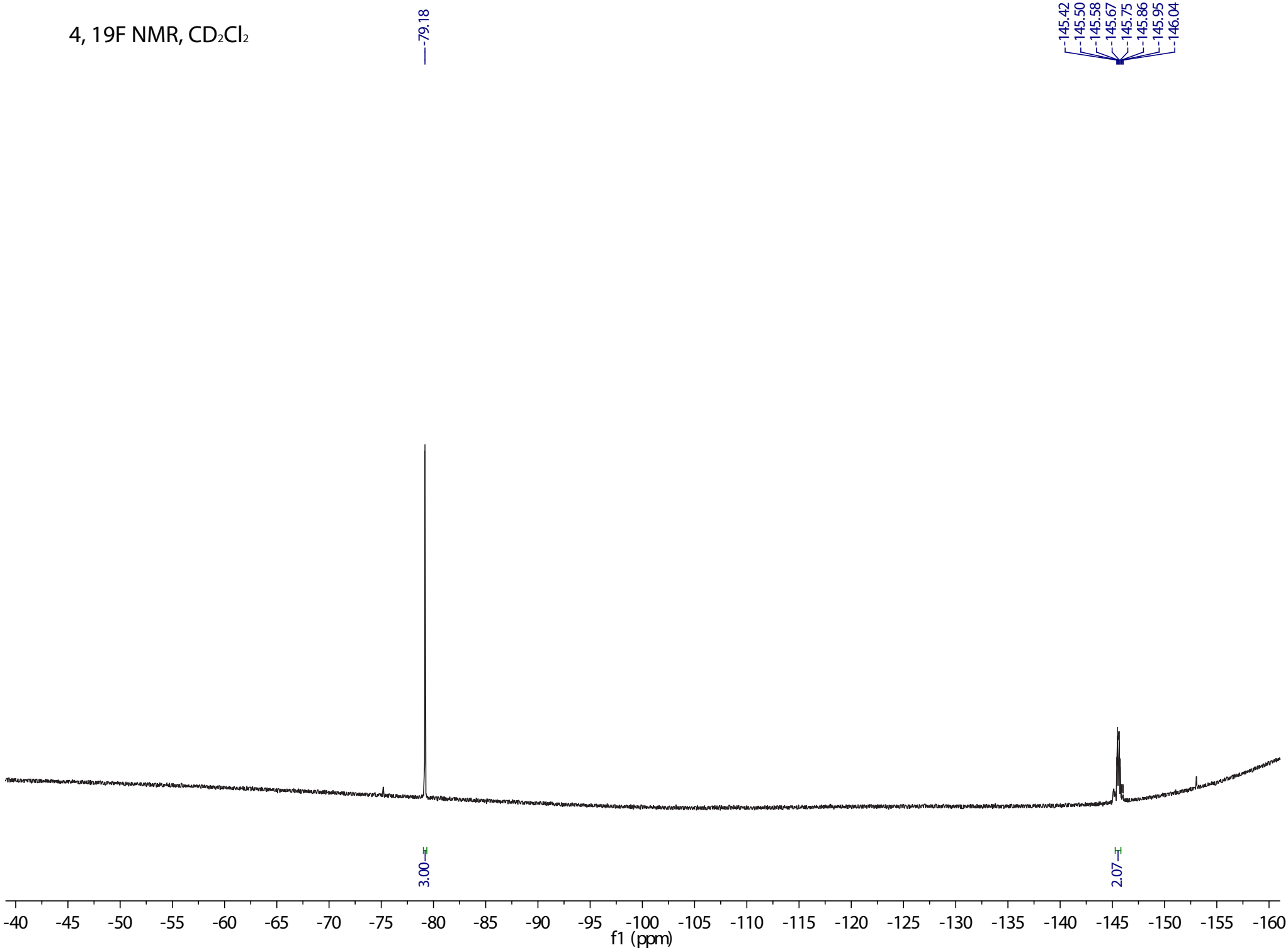

4, 11B{1H} NMR, CD_2Cl_2

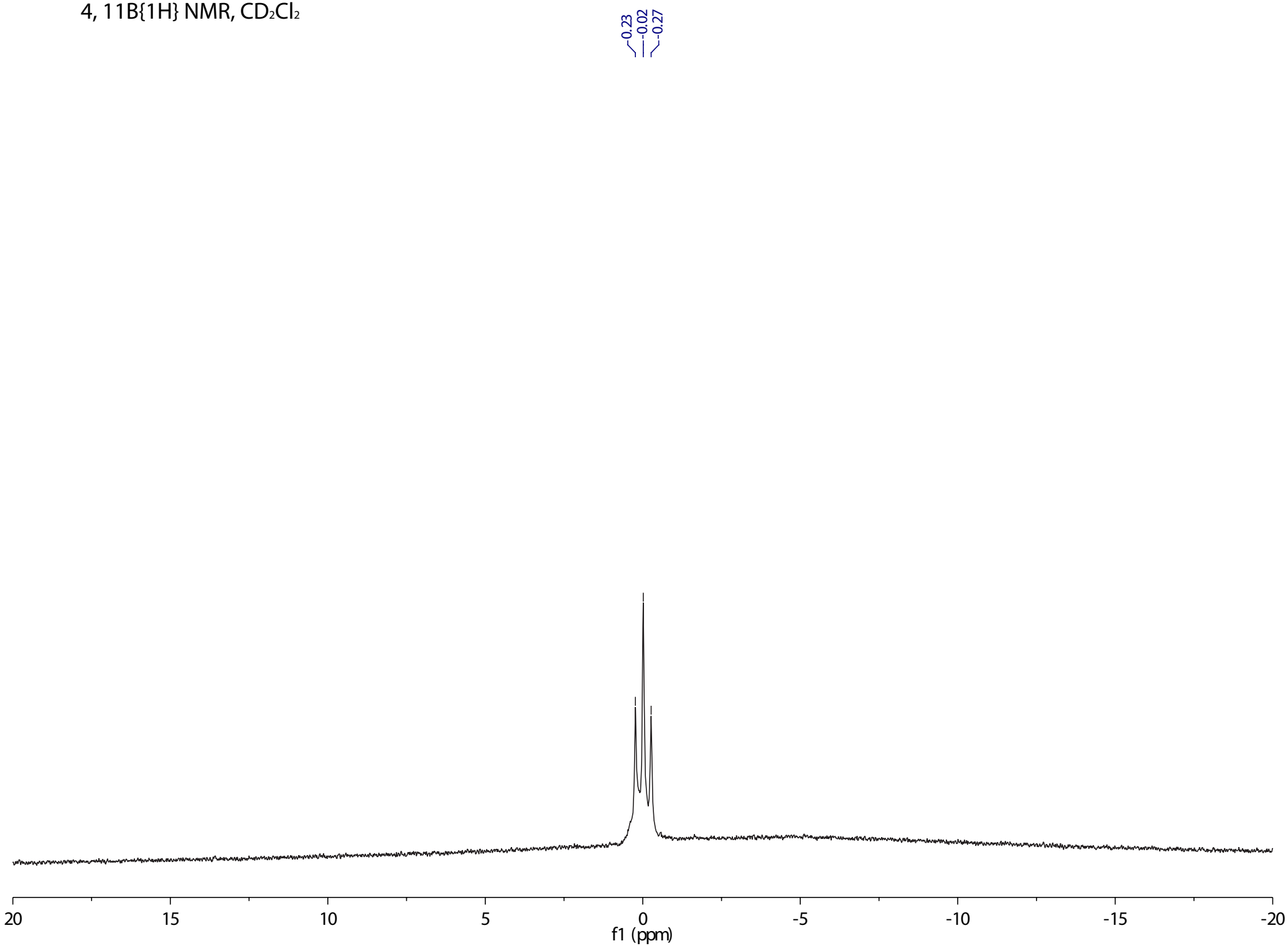

5, 31P{1H} NMR, CD_2Cl_2 + 1 drop CD_3CN

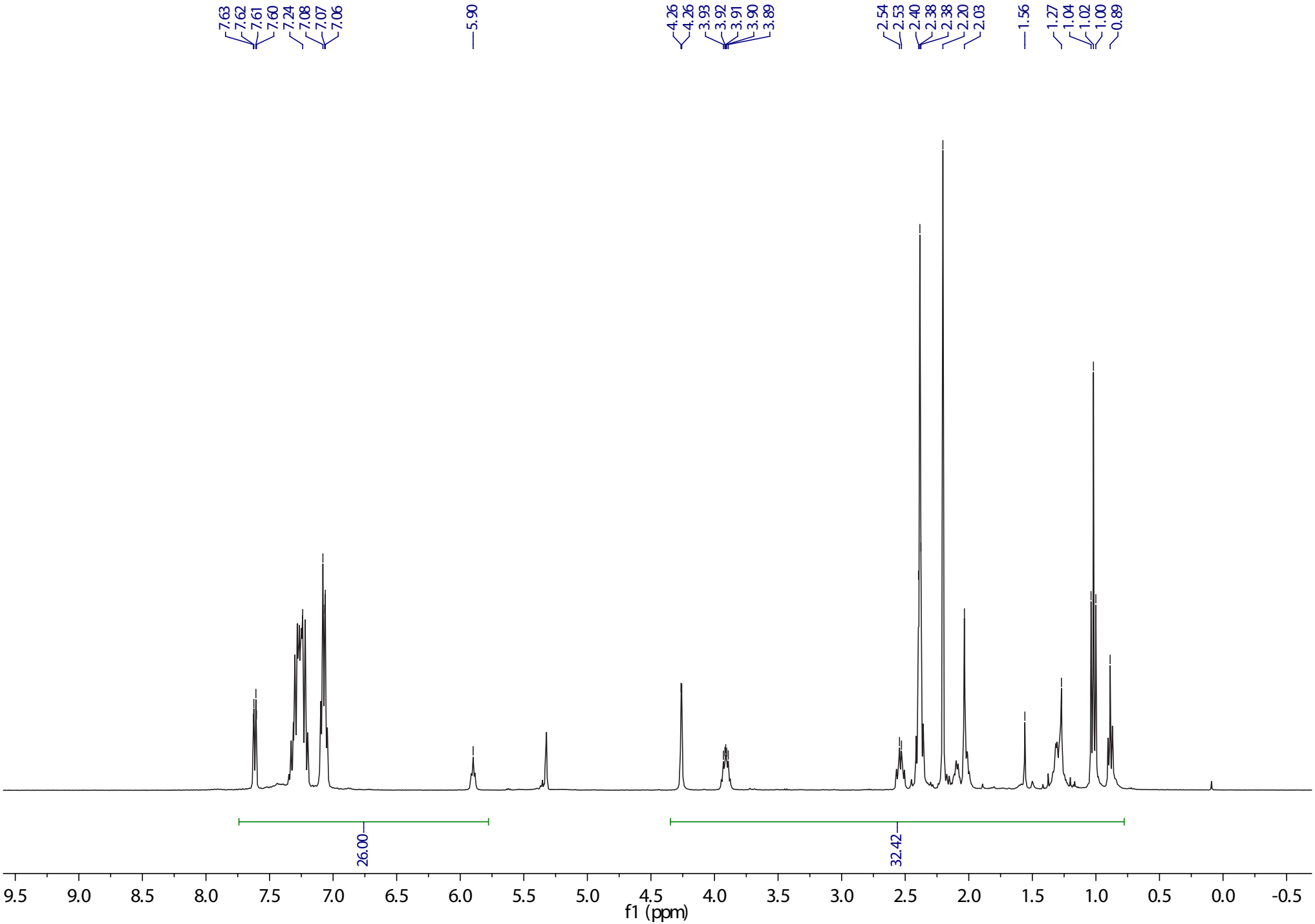

5, 31P{1H} NMR, CD_2Cl_2

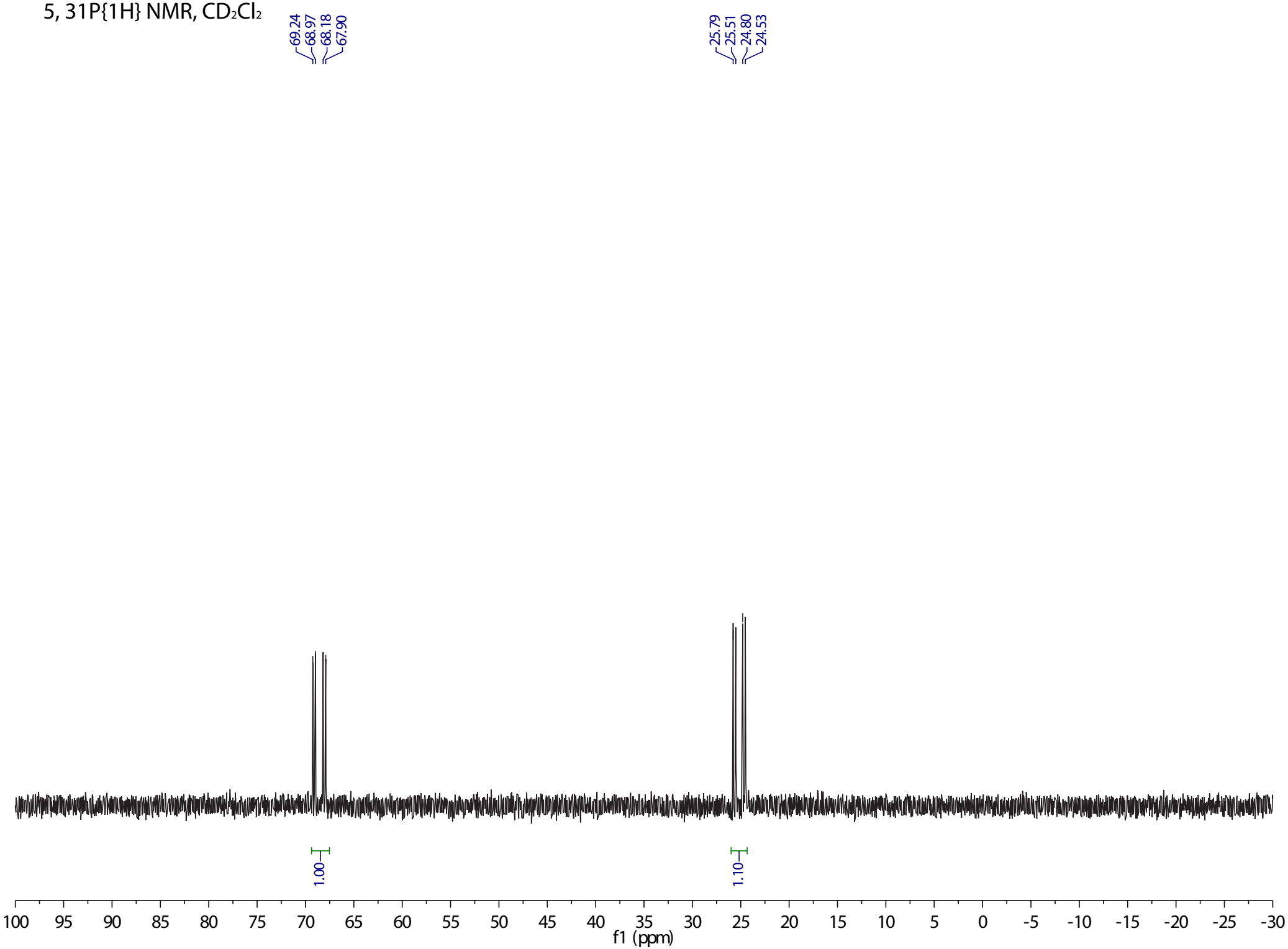

5, 19F NMR, CD_2Cl_2

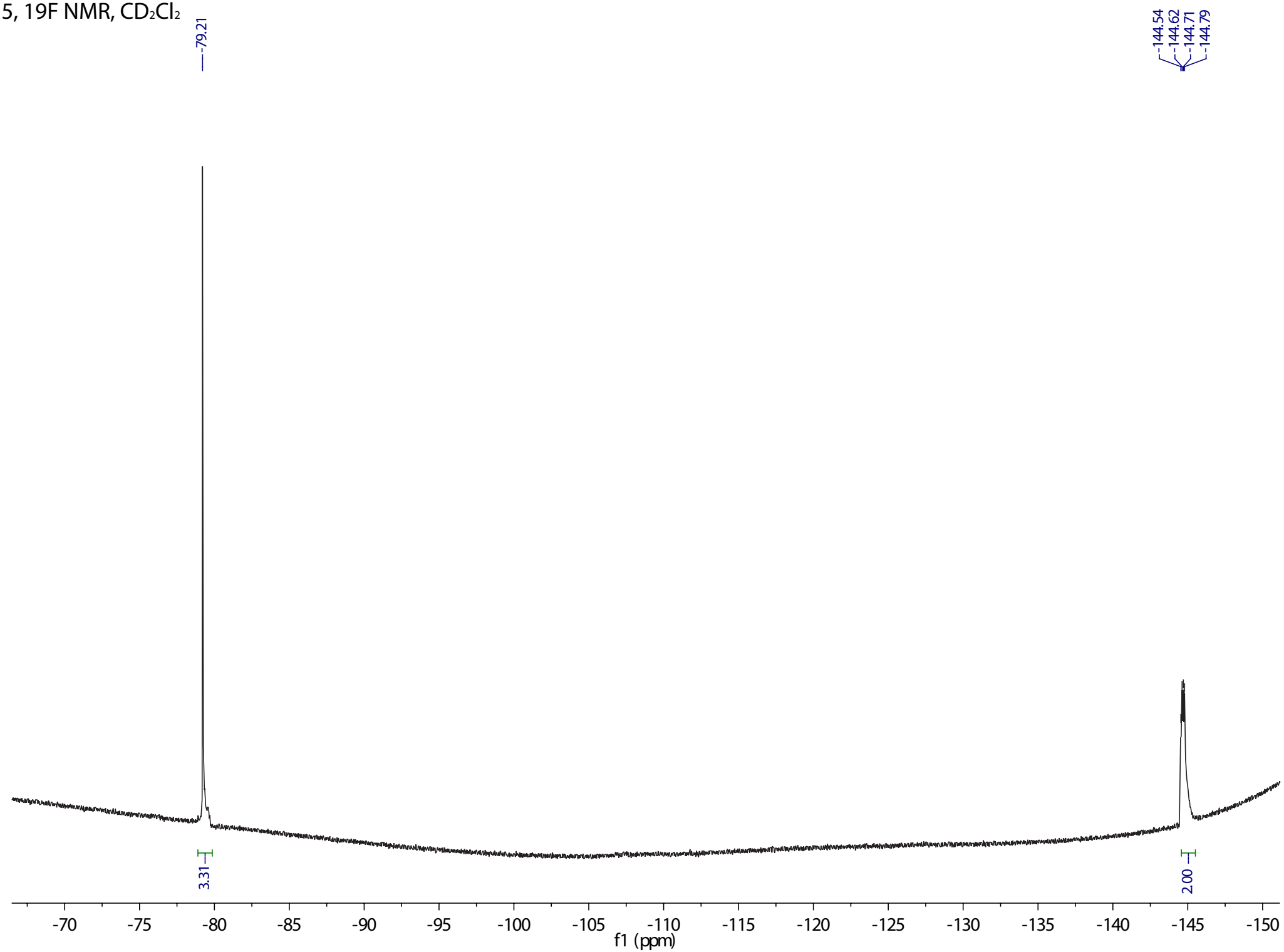

5, 11B{1H} NMR, CD_2Cl_2

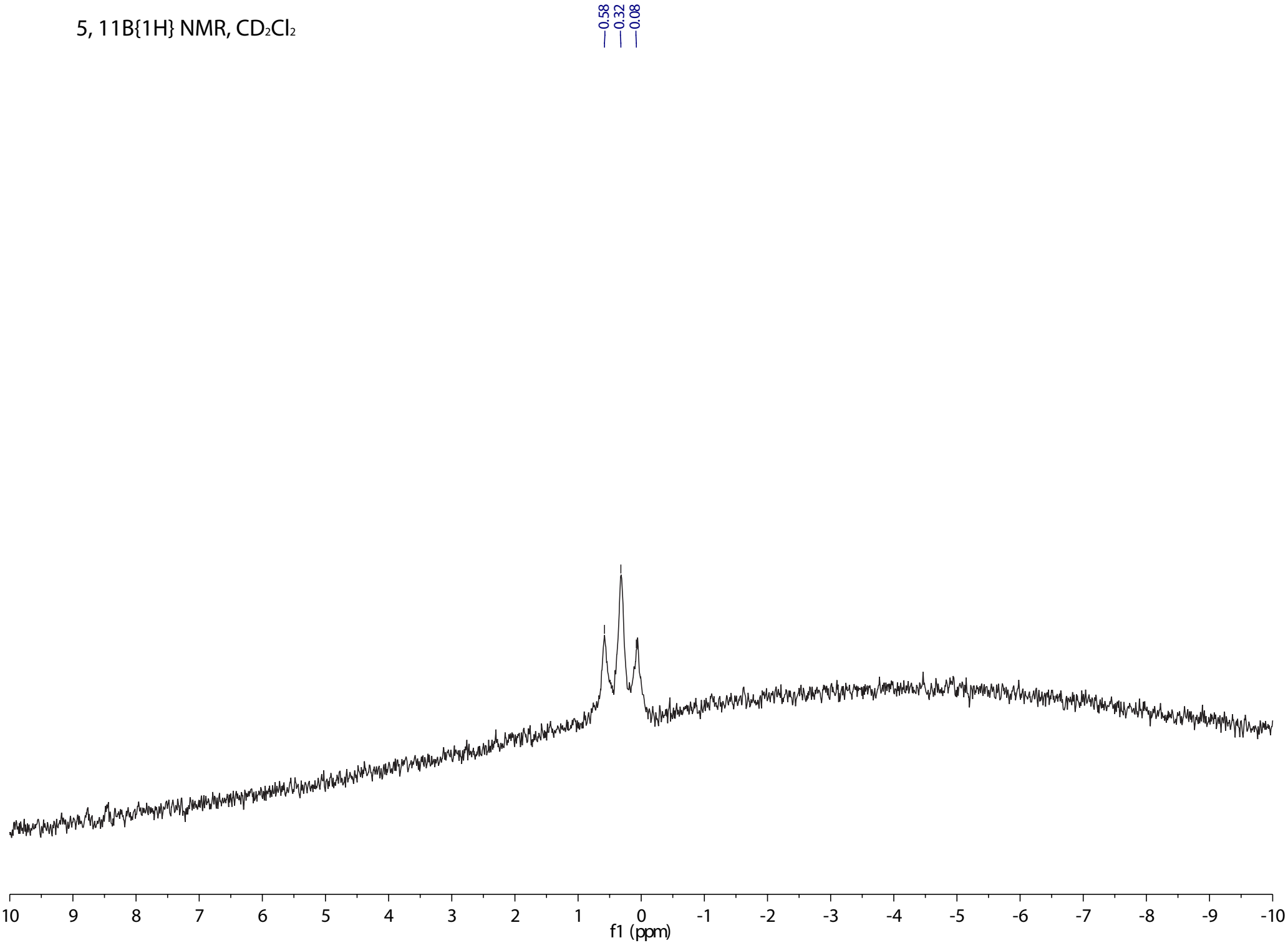

S1, 1H NMR, CD_2Cl_2

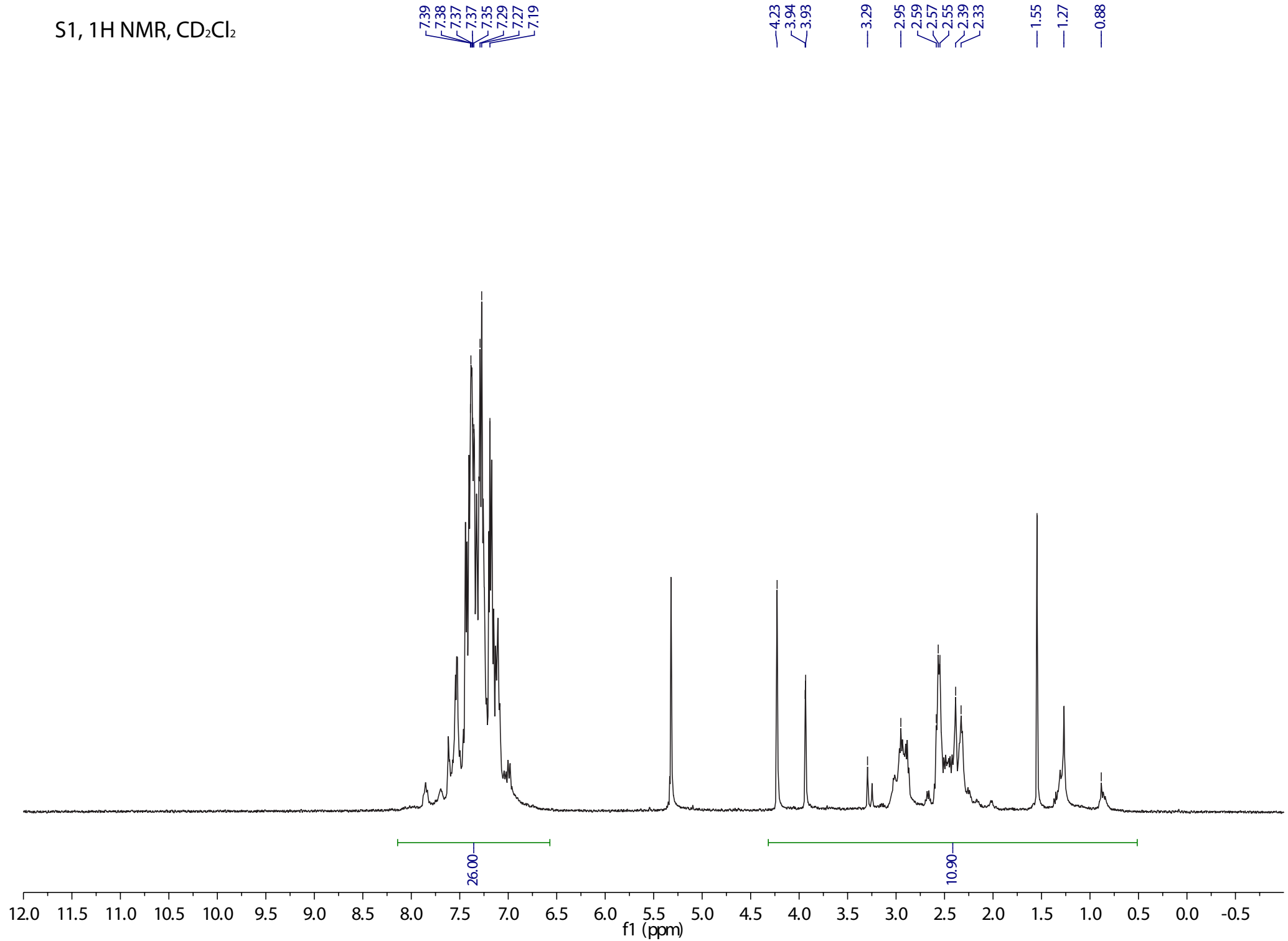

S1, 31P{1H} NMR, CD_2Cl_2

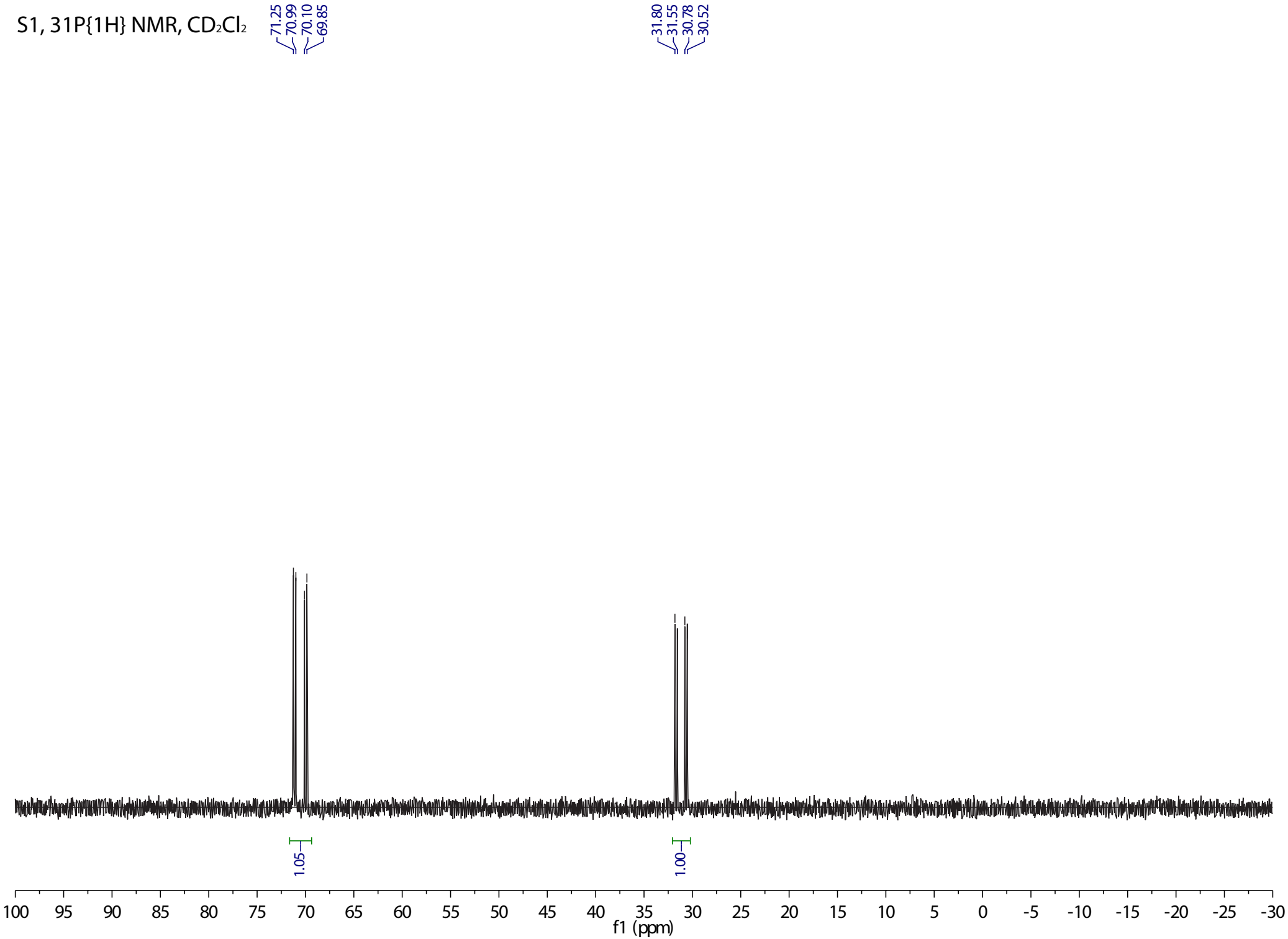

S1, 19F NMR, CD_2Cl_2

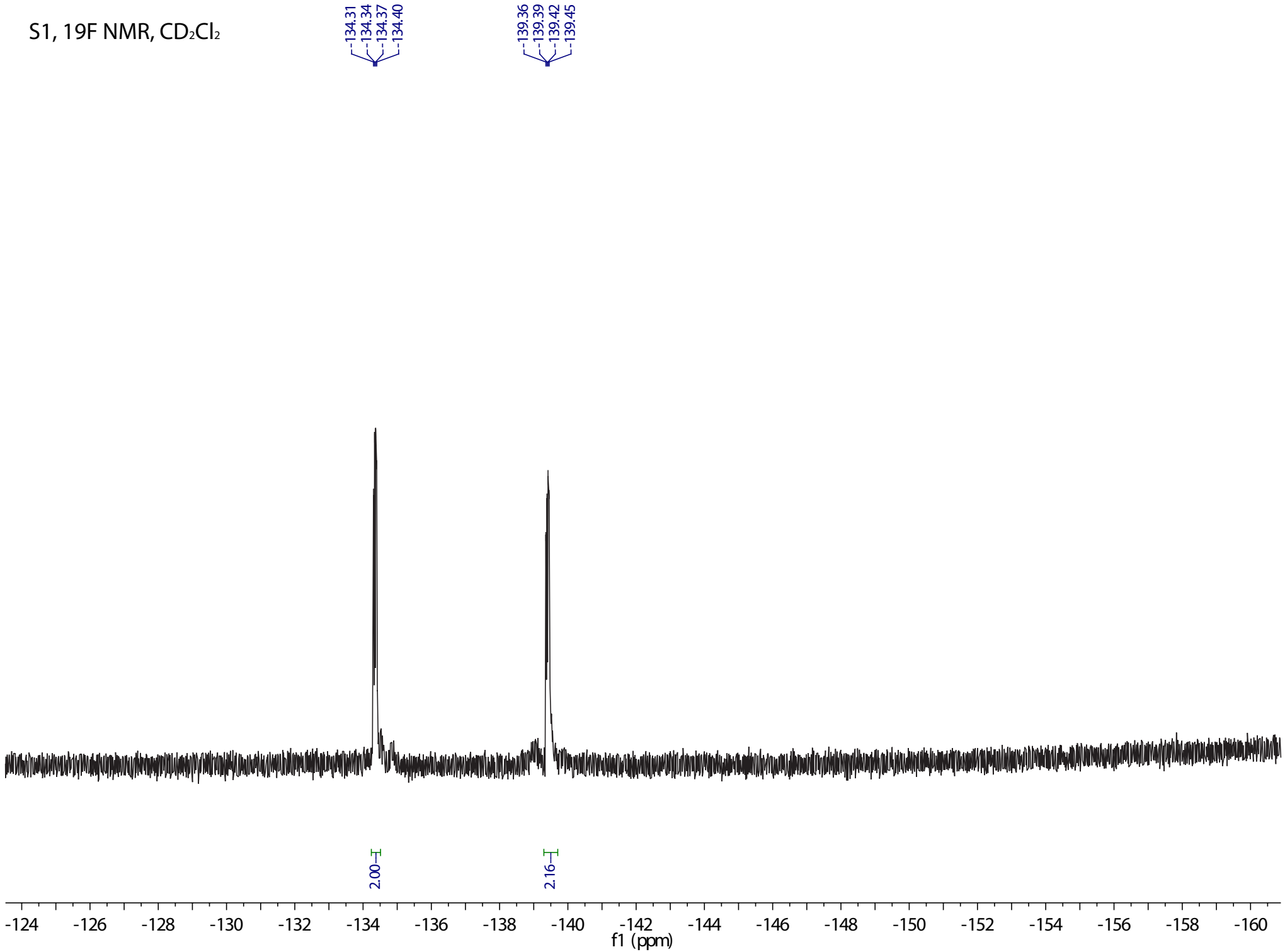

S2, 1H NMR, CD_2Cl_2

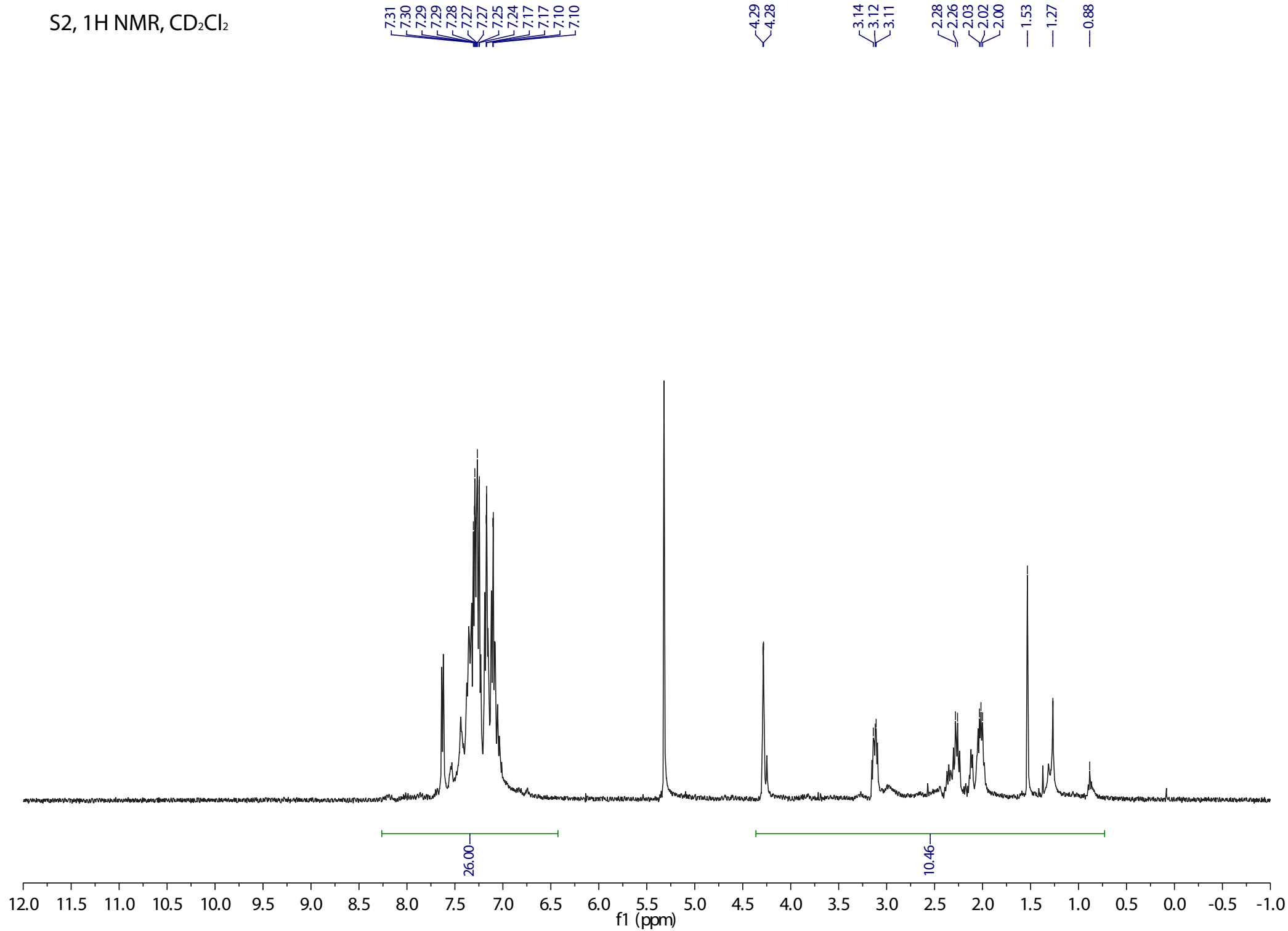

S2, 31P{1H} NMR, CD_2Cl_2

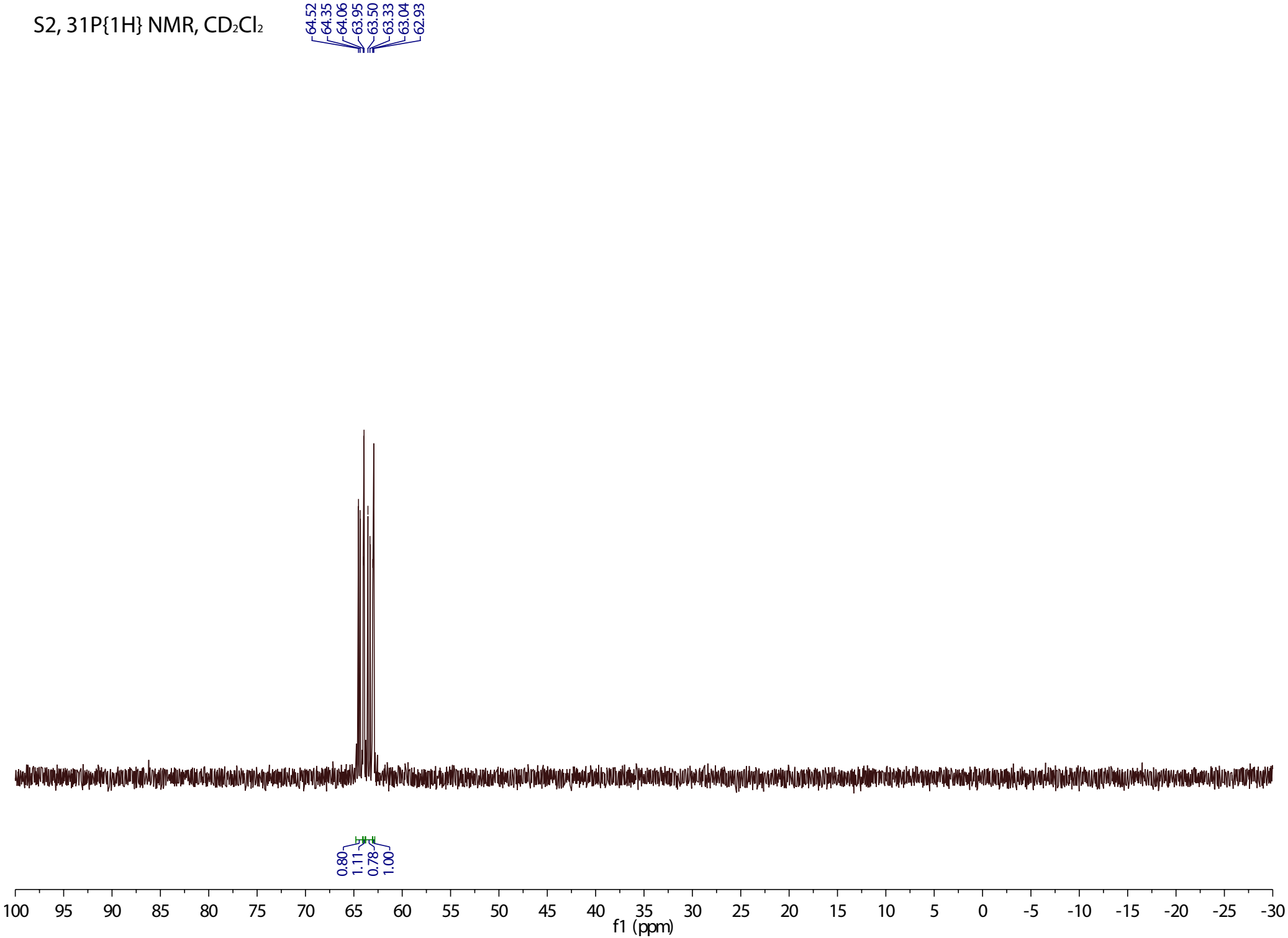

S2, 19F NMR, CD_2Cl_2

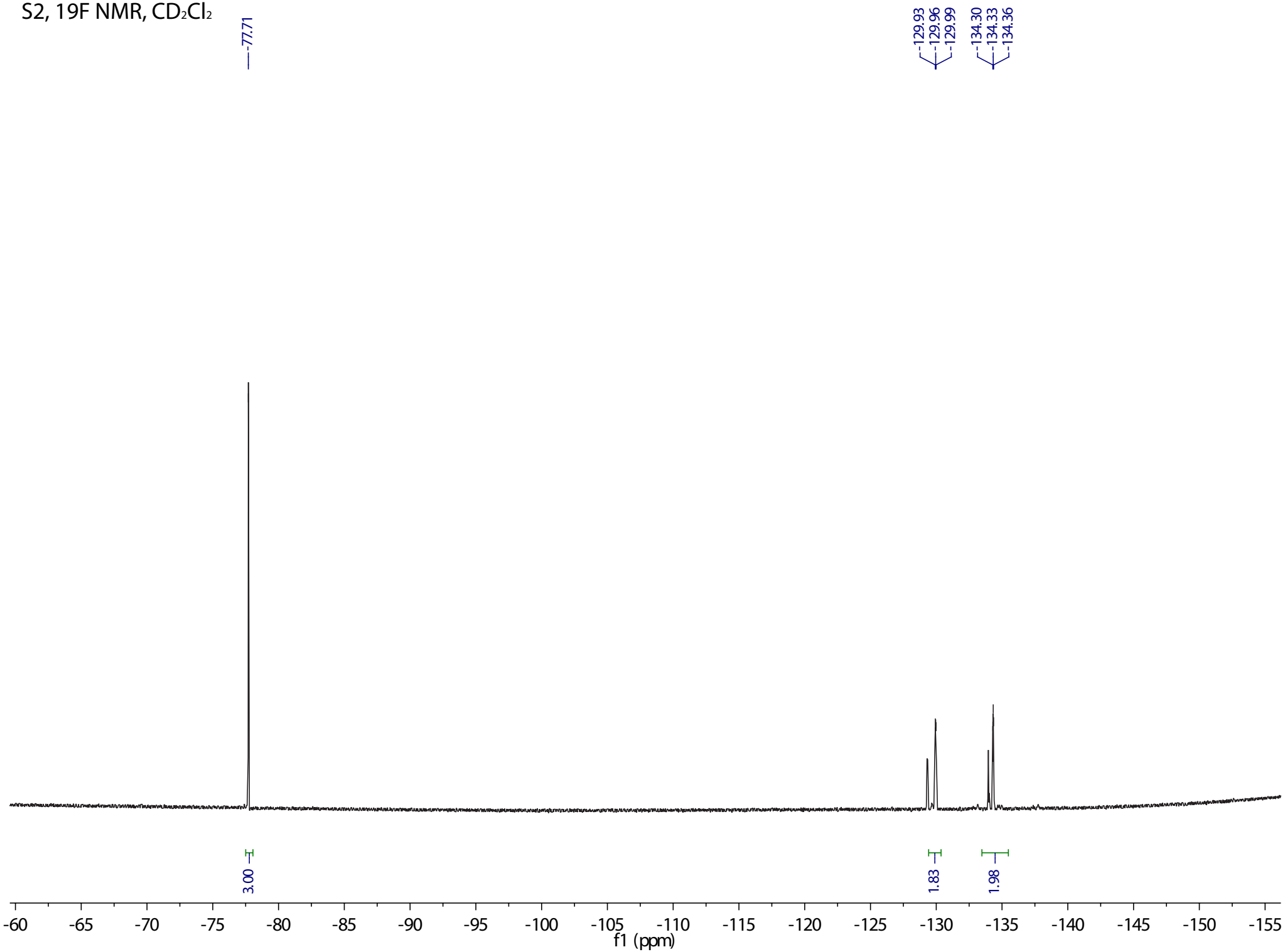

S4, 1H NMR, CD2Cl2

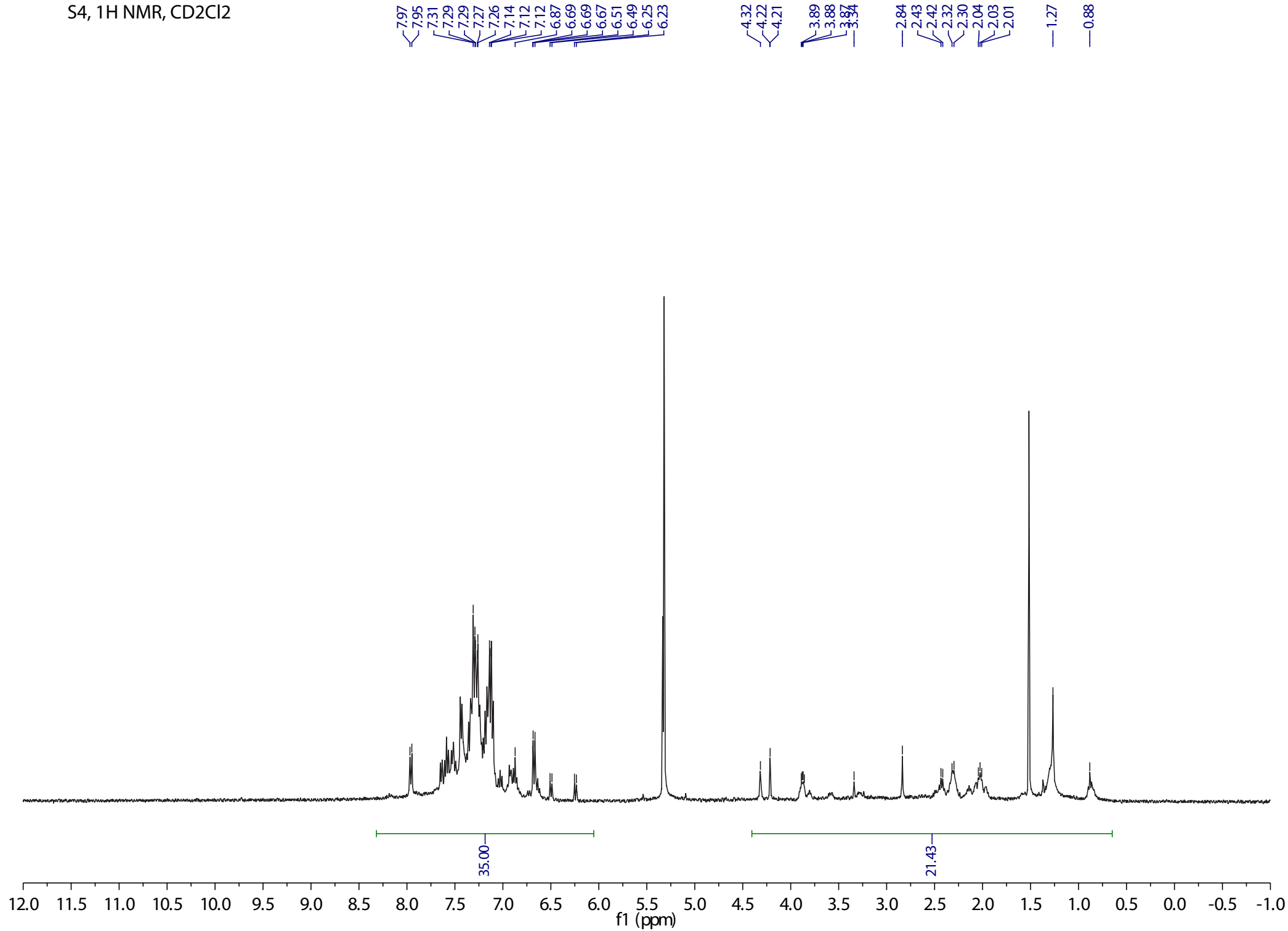

S4, 31P{1H} NMR, CD_2Cl_2

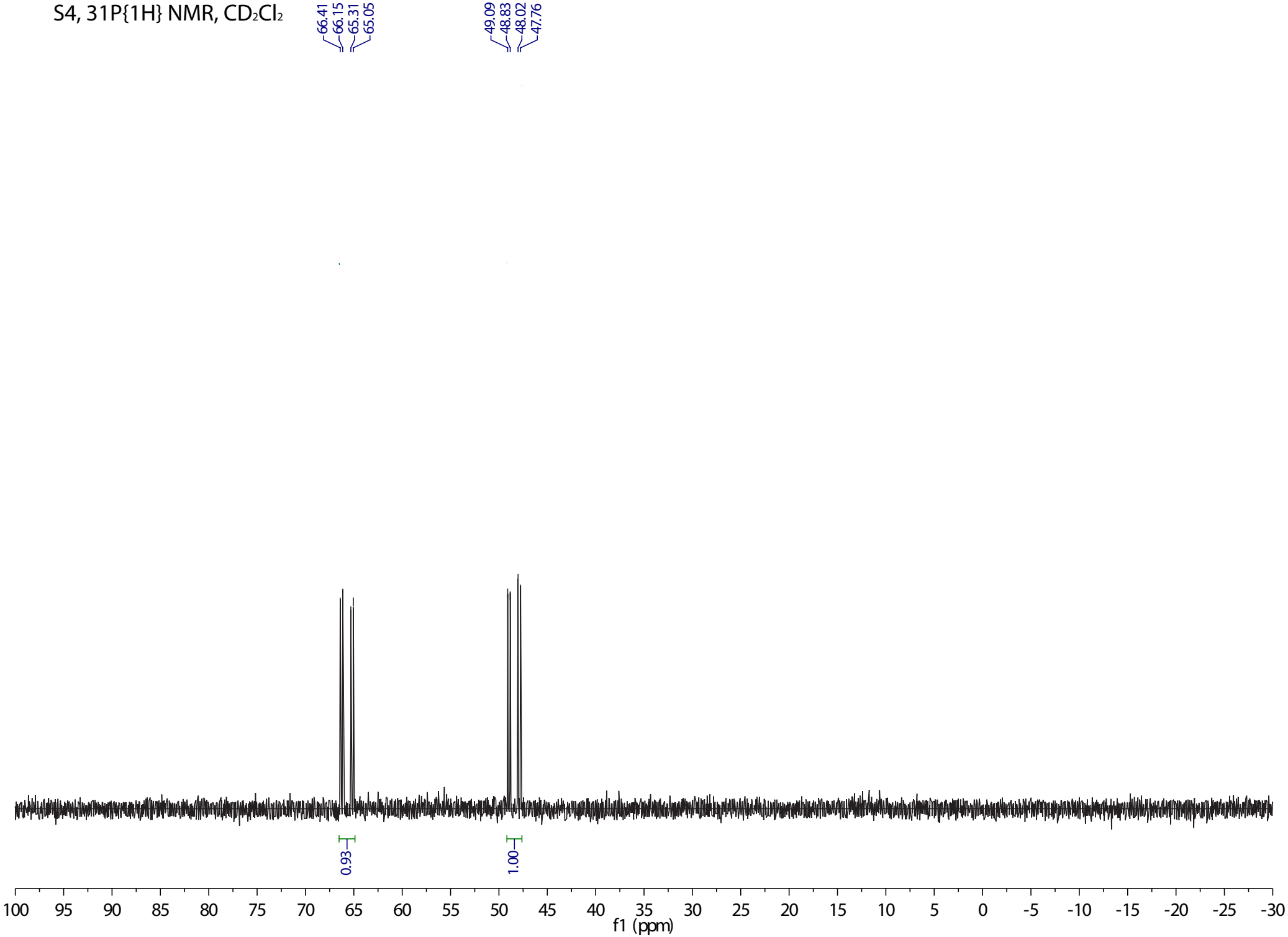

S4, 19F NMR, CD_2Cl_2

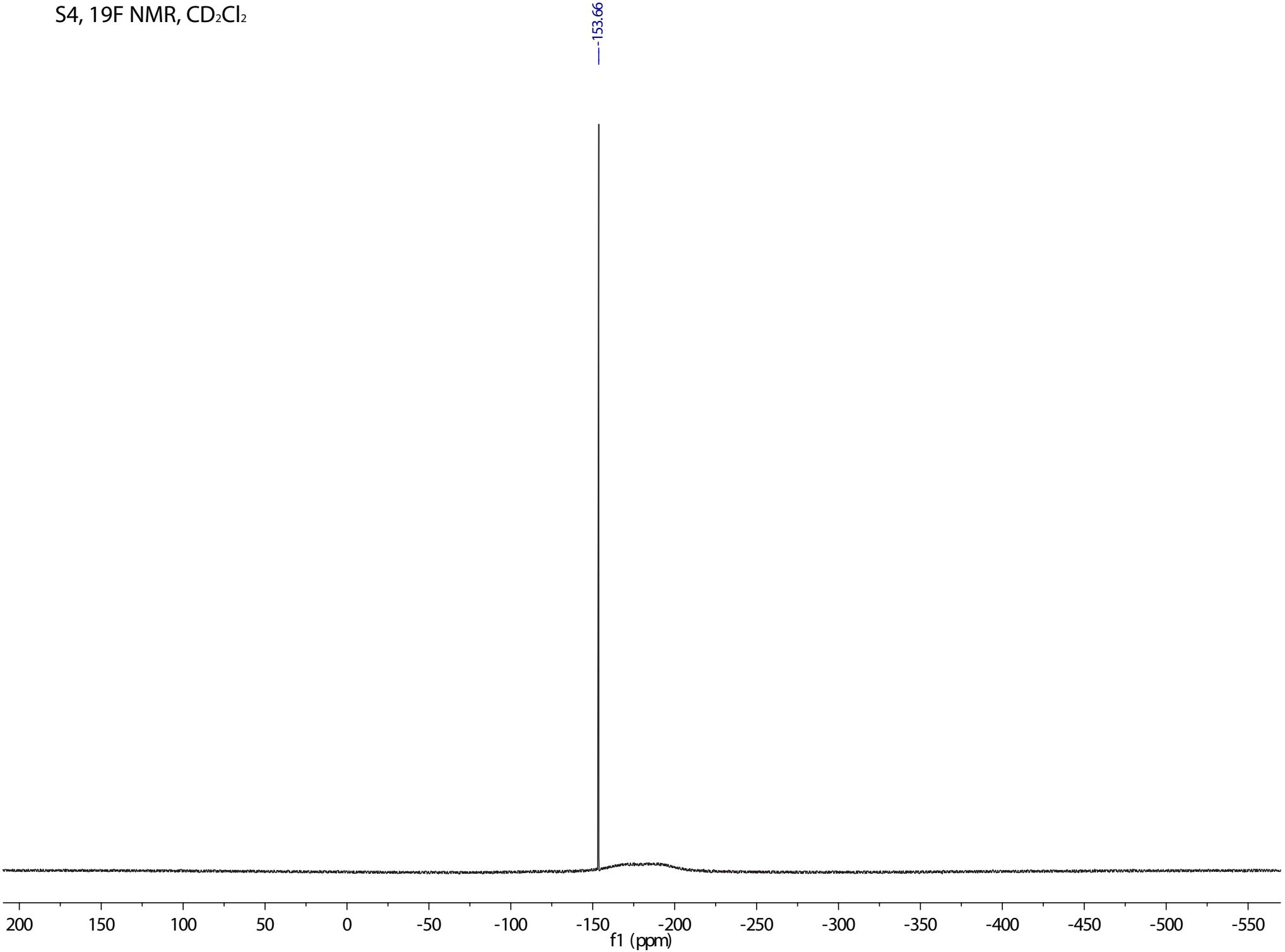

S4, {1H}11B NMR, CD2Cl2

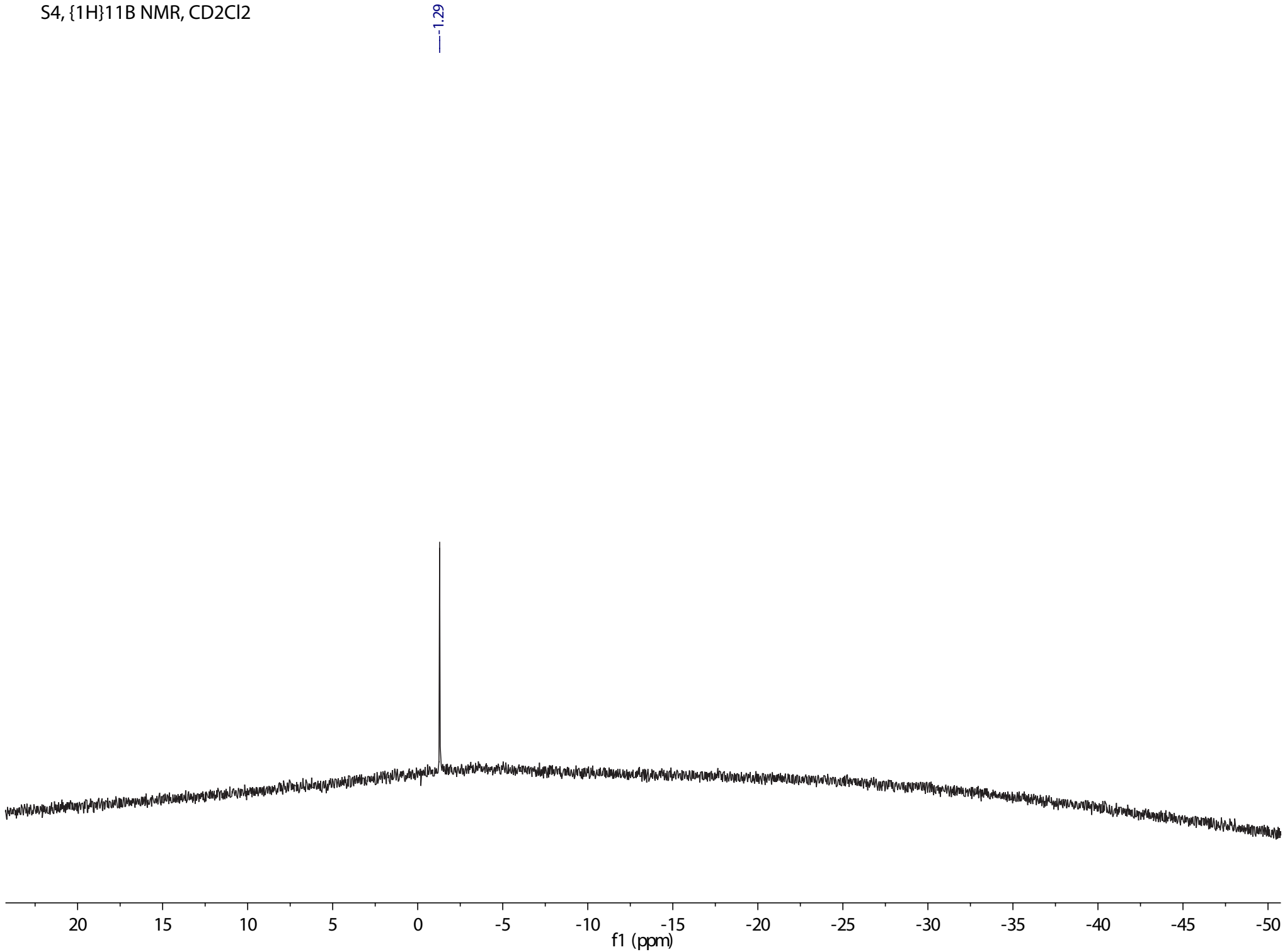

S5, 1H NMR, CD2Cl2 + 1 drop CD3CN

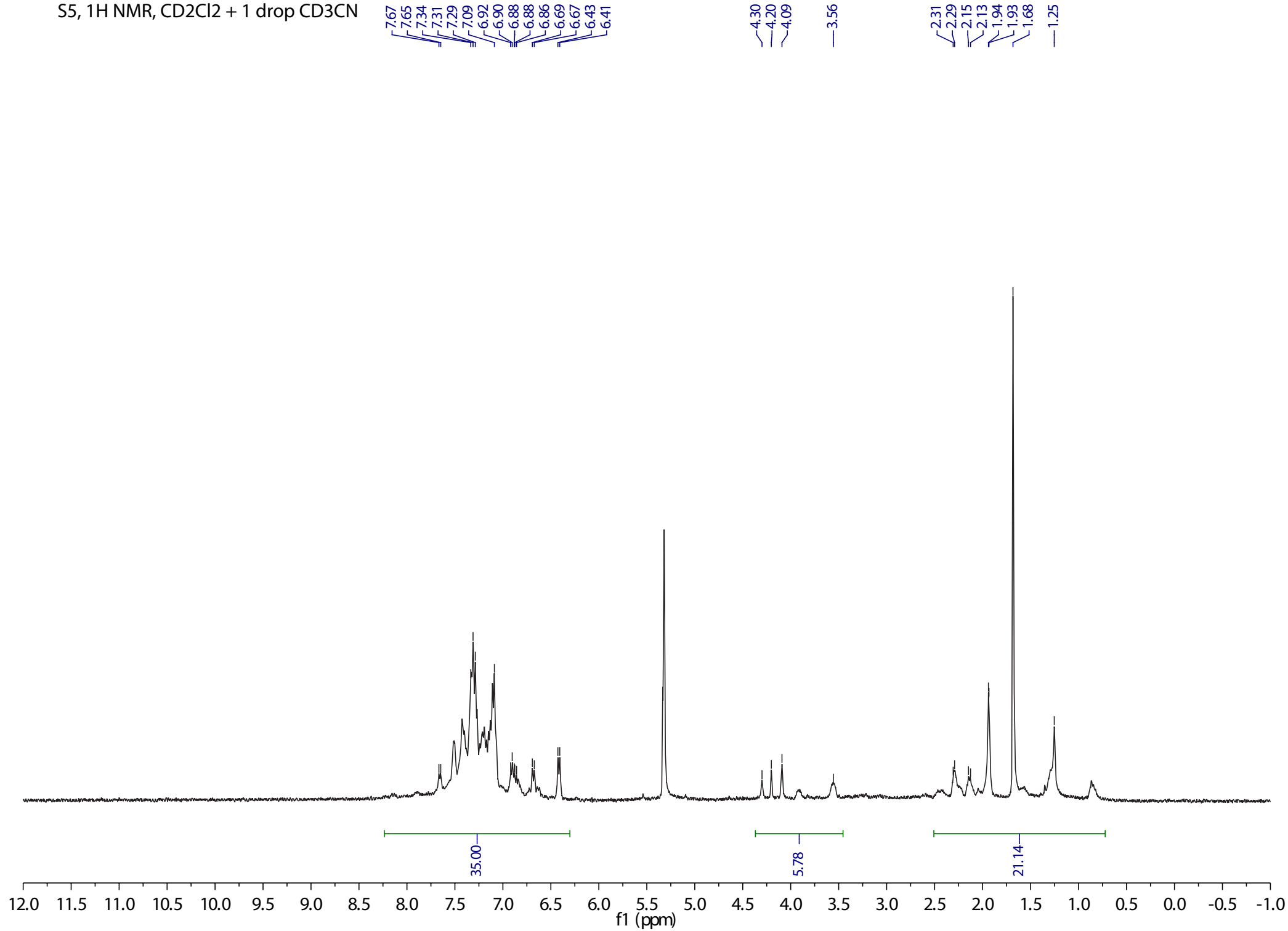

S5, 31P{1H} NMR, CD_2Cl_2

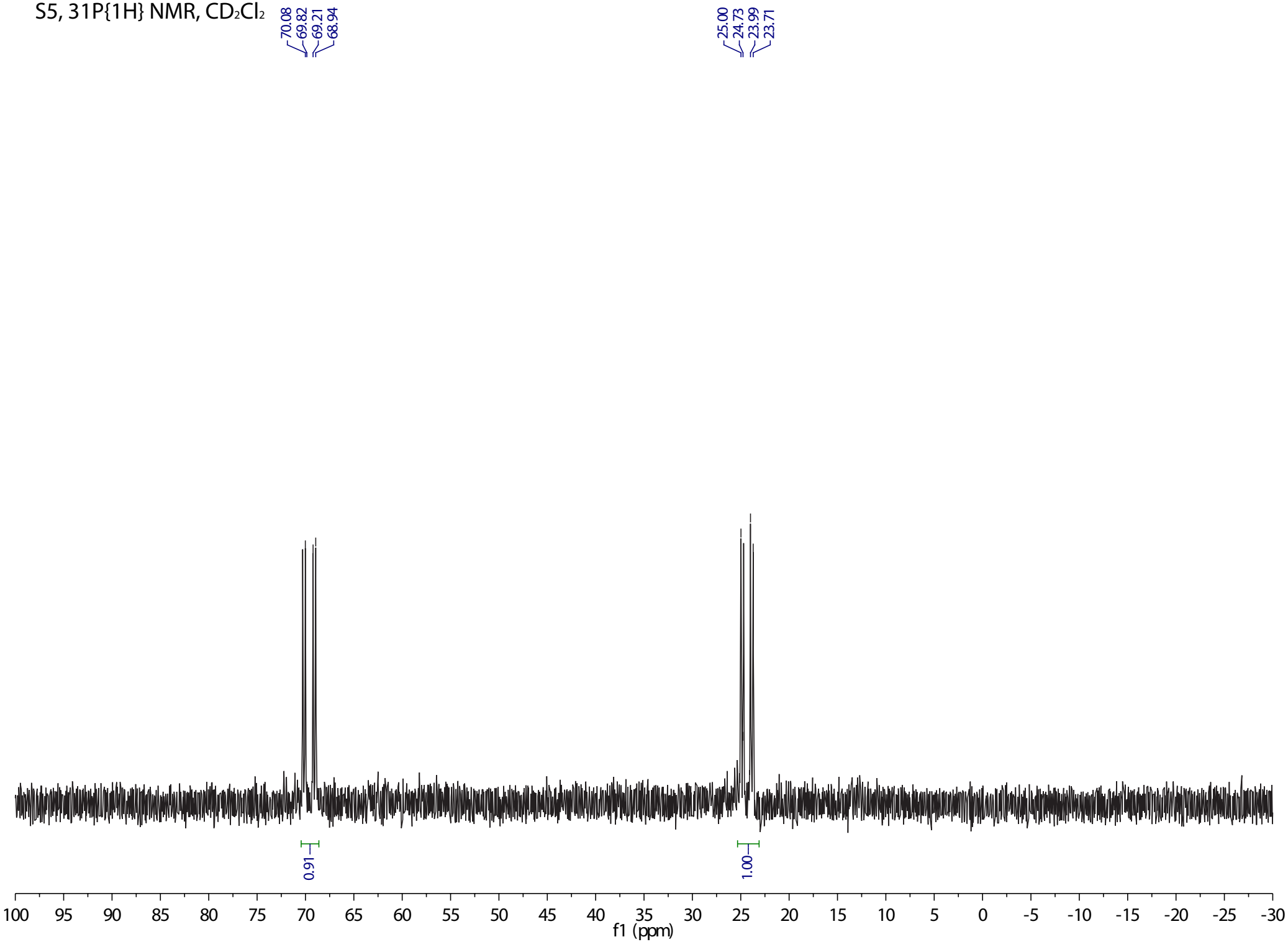

S5, 19F NMR, CD_2Cl_2

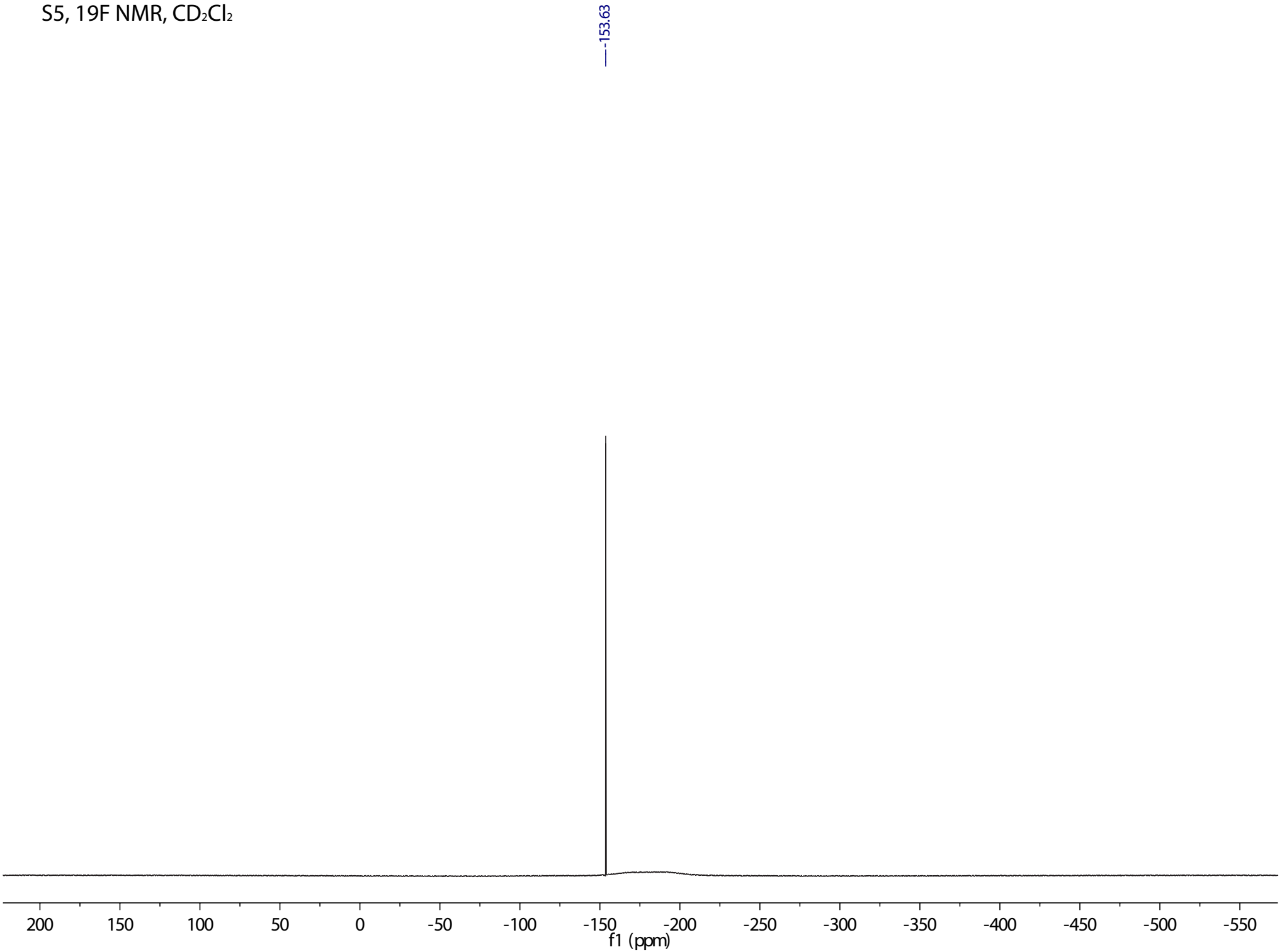

S5, {1H}11B NMR, CD2Cl2

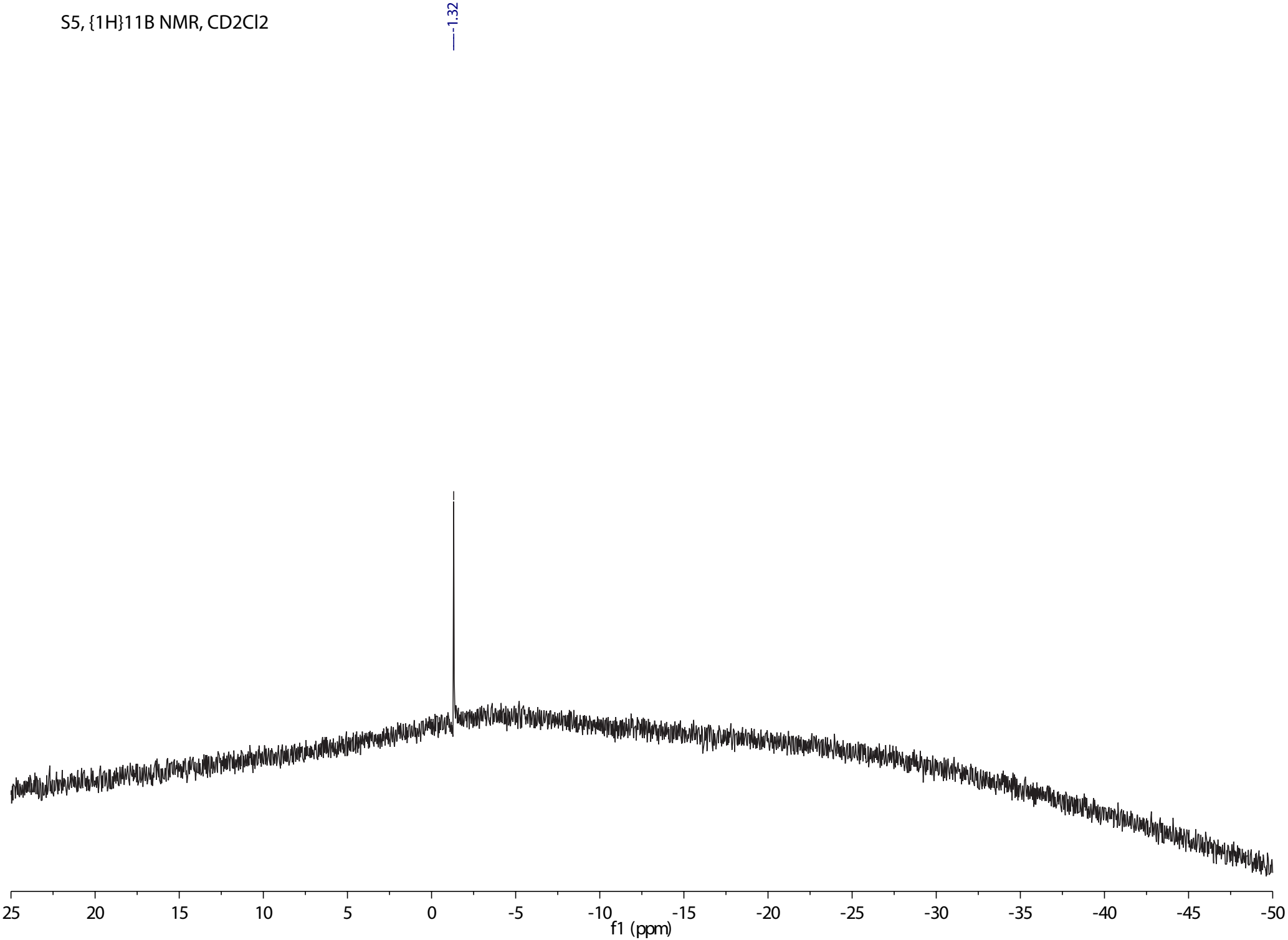

References

1. A. M. Lifschitz, C. M. Shade, A. M. Spokoyny, J. Mendez-Arroyo, C. L. Stern, A. A. Sarjeant and C. A. Mirkin, *Inorg. Chem.*, 2013, **52**, 5484.
2. E. Pfeiffer, M. L. Pasquier and W. Marty, *Helv. Chim. Acta*, 1984, **67**, 654.
3. H. J. Yoon, J. Kuwabara, J. H. Kim and C. A. Mirkin, *Science*, 2010, **330**, 66.
4. R. M. Young, S. M. Dyar, J. C. Barnes, M. Juricek, J. F. Stoddart, D. T. Co and M. R. Wasielewski, *J. Phys. Chem. A*, 2013, **117**, 12438.
5. S. J. Grimme, *Comput. Chem.* 2004, **25**, 1463.
6. M. Ernzerhof and G. Scuseria, *Chem. Phys.* 1999, **110**, 5029.